JOURNAL OF GEOPHYSICAL RESEARCH, VOL. 93, NO. A3, PAGES 1817–1838, MARCH 1, 1988

Satellite Observations of a New Type of Discrete VLF Emission at $L < 4$

W. L. POULSEN AND U. S. INAN

STAR Laboratory, Stanford University, Stanford, California

A new type of discrete whistler mode emission has been observed in the magnetosphere at $L < 4$. The emission elements are confined to a bandwidth of 1–5 kHz, with the lower cutoff frequency of the band varying with L shell, being equal to ~ 0.2–$0.5 f_{Heq}$, where f_{Heq} is the equatorial electron gyrofrequency. The discrete and burstlike nature of the emissions is similar to that of chorus emissions typically observed at higher L; however, dispersion of individual elements is often different from typical chorus, and the emissions are observed inside as well as outside the plasmapause. The phenomenon seems to occur mainly in the early morning local time sector (0400–0800 MLT) and is well correlated with geomagnetic activity, occurring mostly when $\Sigma Kp > 30$. The analysis of data from the low-altitude ISIS 2 and the high-altitude DE 1 satellites indicates that the emissions may be generated near the equatorial plane at frequencies of $\sim 0.2 f_{Heq}$ inside and $\sim 0.35 f_{Heq}$ outside the plasmapause. The parallel energy of electrons for gyroresonance with the observed waves is found to be ~20–50 keV in both cases. Observations in the vicinity of low-altitude crossings of the plasmapause also indicate the presence of a second emission band which is interpreted to result from the reflection of the equatorially generated emissions from the lower ionosphere.

1. INTRODUCTION

A new type of discrete electromagnetic VLF emission has been observed at $L < 4$ in data from the Dynamics Explorer 1 (DE 1) spacecraft as well as from the ISIS 2 and ISEE 1 satellites. In this paper we present the observed characteristics of these emissions: their spectral properties and intensities, occurrence statistics, and observation regions in L shell, geomagnetic latitude, and local time. We also interpret the data in terms of the location of the generation region of the emissions and the energy of the associated gyroresonant energetic particles.

Discrete, spontaneous "chorus" emissions are typically observed predominantly outside the plasmapause [*Tsurutani and Smith*, 1974; *Burtis and Helliwell*, 1976], whereas plasmaspheric hiss and mid-latitude hiss are observed primarily within the plasmasphere [*Thorne et al.*, 1973]. Satellite observations show a relatively abrupt termination of chorus activity at the plasmapause boundary [*Anderson and Gurnett*, 1973]. Chorus emissions often occur in bands, predominantly at normalized frequencies of $f/f_H \simeq 0.2$–0.45 and 0.55–0.65 with a distinct gap at $f/f_H = 0.5$, where f_H is the electron gyrofrequency [*Burtis and Helliwell*, 1976]; such features of terrestrial chorus are also remarkably reproduced by Jovian VLF chorus observed on the Voyager 1 and 2 satellites [*Inan et al.*, 1983; *Coroniti et al.*, 1984]. Magnetospheric chorus is typically found at $L > 4$, is correlated with geomagnetic activity, occurs mainly from 0300 to 1500 MLT, moves to lower L during geomagnetic disturbances, and is believed to propagate on nonducted ray paths that deviate inward to lower L shells with increasing distance from the hypothesized equatorial generation region [*Burtis and Helliwell*, 1976]. The emission described herein has many similar characteristics, and may be an extension of such chorus to lower L and higher frequencies during periods when the plasmapause moves inward to $L < 3$ because of high geomagnetic activity ($\Sigma Kp > 30$). However, it is also observed inside the plasmasphere, occurs in a more restricted local time period (0400–0800 MLT), and is much better correlated with geomagnetic activity. Furthermore, individual emission elements exhibit dispersion properties that differ from those of typical chorus.

Discrete choruslike emissions of the kind reported in this paper have been observed in previous satellite VLF data acquired inside the plasmapause. For example, Figure 1 of *Carpenter et al.* [1968] shows a good example of this type of emission observed on the Alouette 1 satellite, with spectral characteristics as well as local time of observation similar to those described in this paper. However, *Carpenter et al.* [1968] emphasized the whistler occurrence rate inside and outside the plasmasphere and did not discuss the discrete emissions.

A preliminary version of the results presented in this paper was reported earlier by *Poulsen and Inan* [1985]. Since that time, observations of the same phenomenon on the Interkosmos satellites have been reported [*Boskova et al.*, 1987].

2. OBSERVATIONS ON THE HIGH-ALTITUDE DE 1 AND THE LOW-ALTITUDE ISIS 2 SATELLITES

In this section, we discuss the characteristics of the discrete VLF emissions as observed on the high-altitude DE 1 and the low-altitude ISIS 2 satellites, including (1) spectral properties, (2) occurrence characteristics versus invariant latitude (L shell) and local time, (3) distribution in geomagnetic latitude, (4) electric and magnetic field intensities, (5) relationship to geomagnetic activity, and (6) relationship to plasmapause location.

The DE 1 data were acquired using a combination of two receivers, the Stanford University linear wideband receiver (LWR) operating in the 10- to 16-kHz range and the Uni-

Paper number 6A8879.
0148-0227/88/006A-8879$05.00

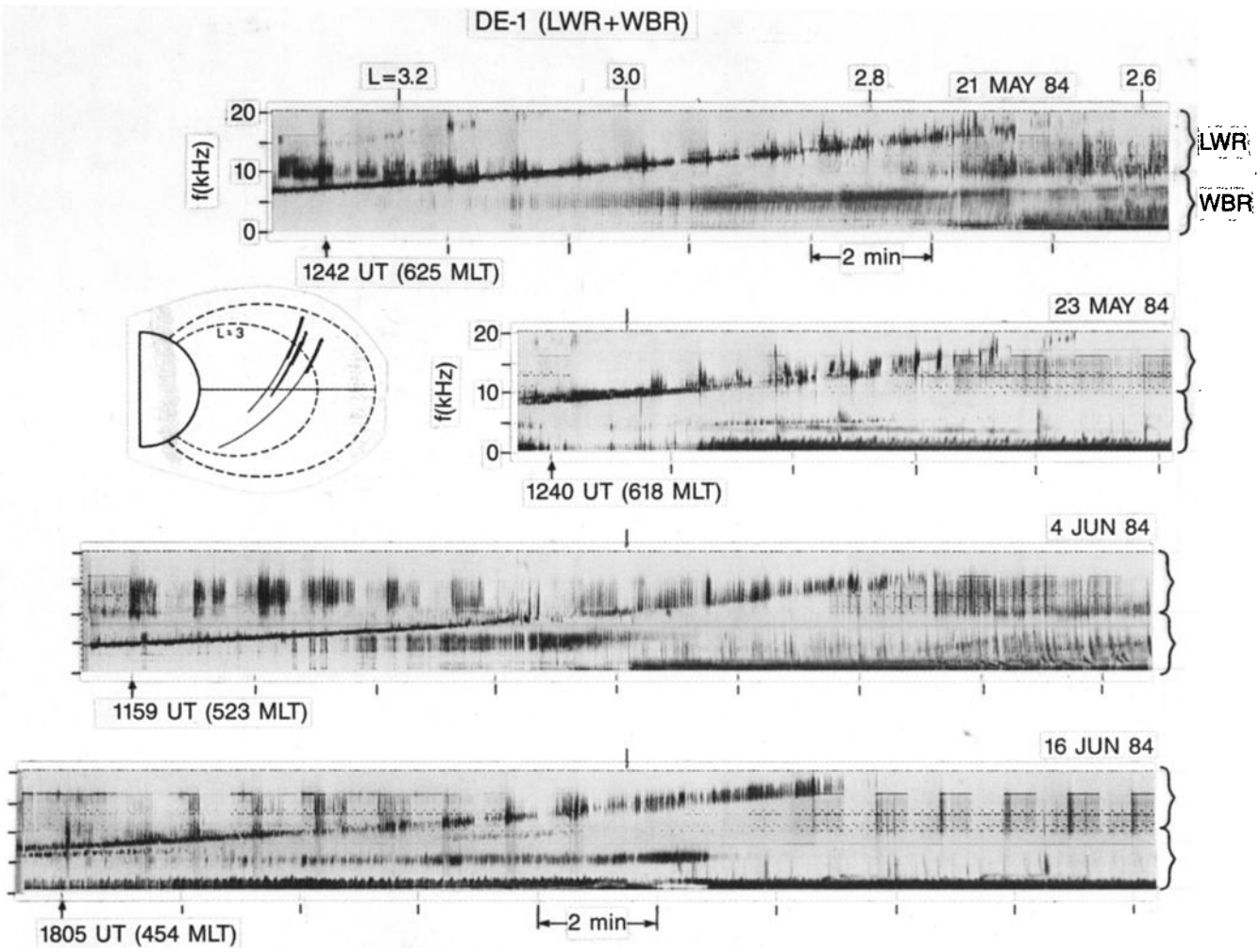

Fig. 1. Examples of discrete emission bands observed on the high-altitude DE 1 satellite. Data from four different periods in which the DE 1 orbital configuration was similar are shown. The orbital segments for each day are indicated in the inset; the darker portions indicate the regions where the discrete emission bands were observed. The L shell for the May 21, 1984, pass is indicated on top of the spectrogram. The spectra from the other days are aligned with the top panel on the basis of the $L = 3$ crossing. The variation of the emission band frequency with L shell is similar on all four days shown. All four days represent data acquired in the early morning local time sector (0400–0700 MLT). In all cases shown, the LWR was toggled between the E_x and B antennas every 32 s. The 600-Hz to 10-kHz portion of each spectrogram in this figure, as well as in Figures 2 and 7, is obtained from the WBR, while the 10- to 20-kHz portion is obtained from the LWR. (The LWR has a steep roll-off above 16 kHz (~ 10 dB down at 17 kHz).)

versity of Iowa wideband receiver (WBR) operating in the 600-Hz to 10-kHz range. The WBR has logarithmic response with rapid (< 1 s) automatic gain control (AGC) over the band, while the LWR has linear amplitude response at fixed gain levels that can automatically change at 8-s intervals [*Shawhan et al.*, 1981]. At all times shown for the DE 1 data in this paper, the LWR was toggled at 32-s intervals between the electric dipole (E_x) and magnetic loop (B) antennas. The DE 1 satellite has a spin period of 6 s, which causes a 3-s (half-period) spin fading modulation in most of the DE 1 spectrograms shown in this paper. (This effect is most clearly visible in the expanded record of Figure 8.)

The ISIS 2 satellite is in an approximately circular orbit at ~1400 km altitude and is equipped with a broadband wave receiver covering the 10-Hz to 25-kHz range and coupled to a 75-m (tip-to-tip) electric dipole antenna [*Franklin et al.*, 1960; *Florida*, 1969]. The receiver gain across the entire frequency range is continuously adjusted with rapid (< 1 s) AGC. The ISIS 2 satellite data were made available to us by courtesy of G. James, Communications Research Centre, Ottawa, Canada. The data acquisition was carried out during 1982–1983 at Siple Station, Antarctica, in support of VLF wave injection experiments [*Helliwell and Katsufrakis*, 1978]. Data acquired at Ottawa during 1980 and 1981 are also used.

Spectral Properties; DE 1 Observations

Figure 1 shows frequency-time records from four different days on which the discrete emission bands were observed on the DE 1 satellite. The satellite locations in all four cases shown were similar; orbital segments corresponding to the times of the data are indicated in the inset plot. The portion of the orbit during which the emissions were observed is marked with a heavier line.

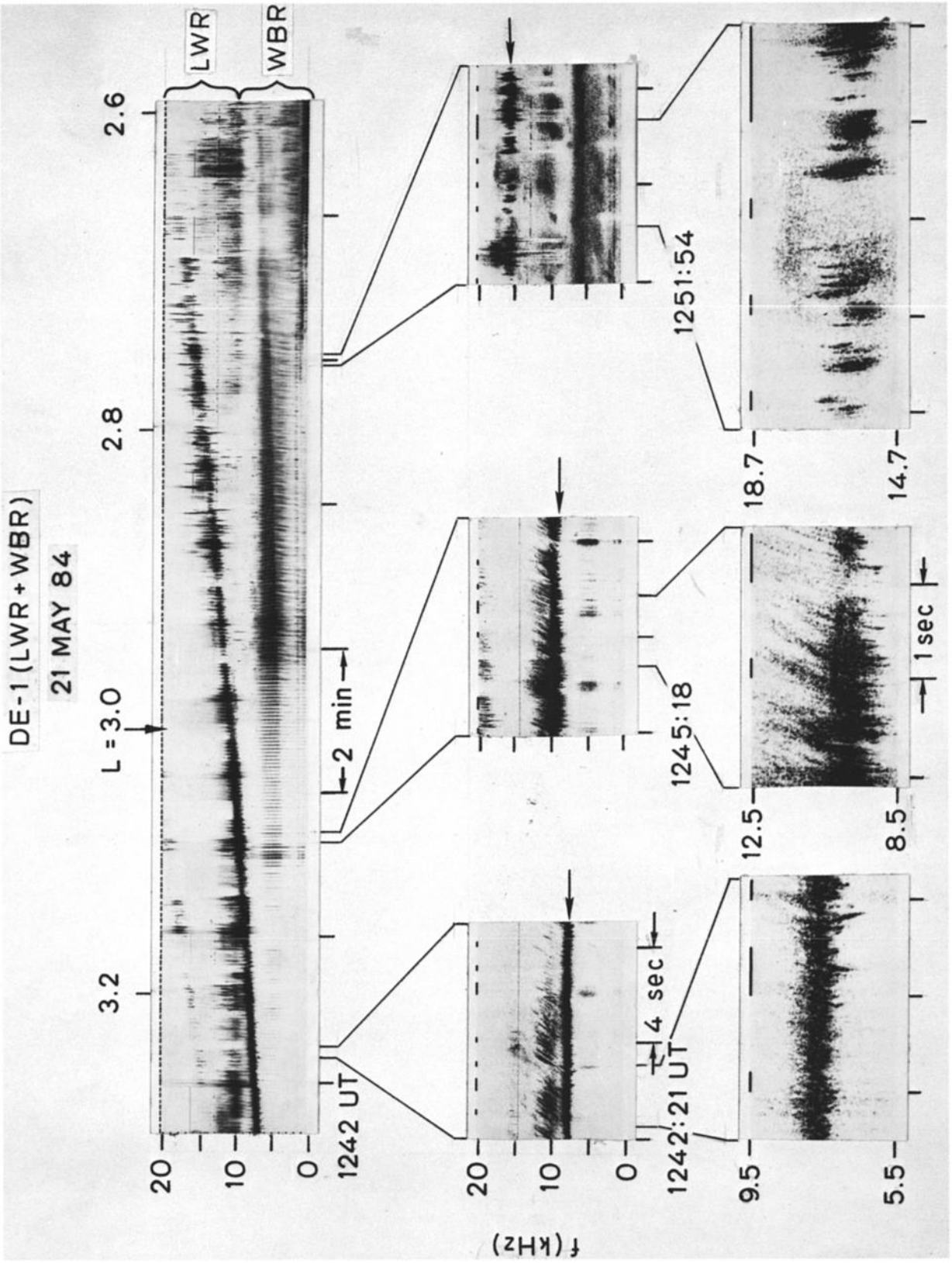

Fig. 2. Expanded spectra showing the discrete emission elements in detail at three different locations. In the middle panel, the emission band is indicated with an arrow. The lowest panel shows that the dispersion of individual emission elements is quite different from the typical "risers" and "fallers" of magnetospheric chorus [*Burtis and Helliwell*, 1976].

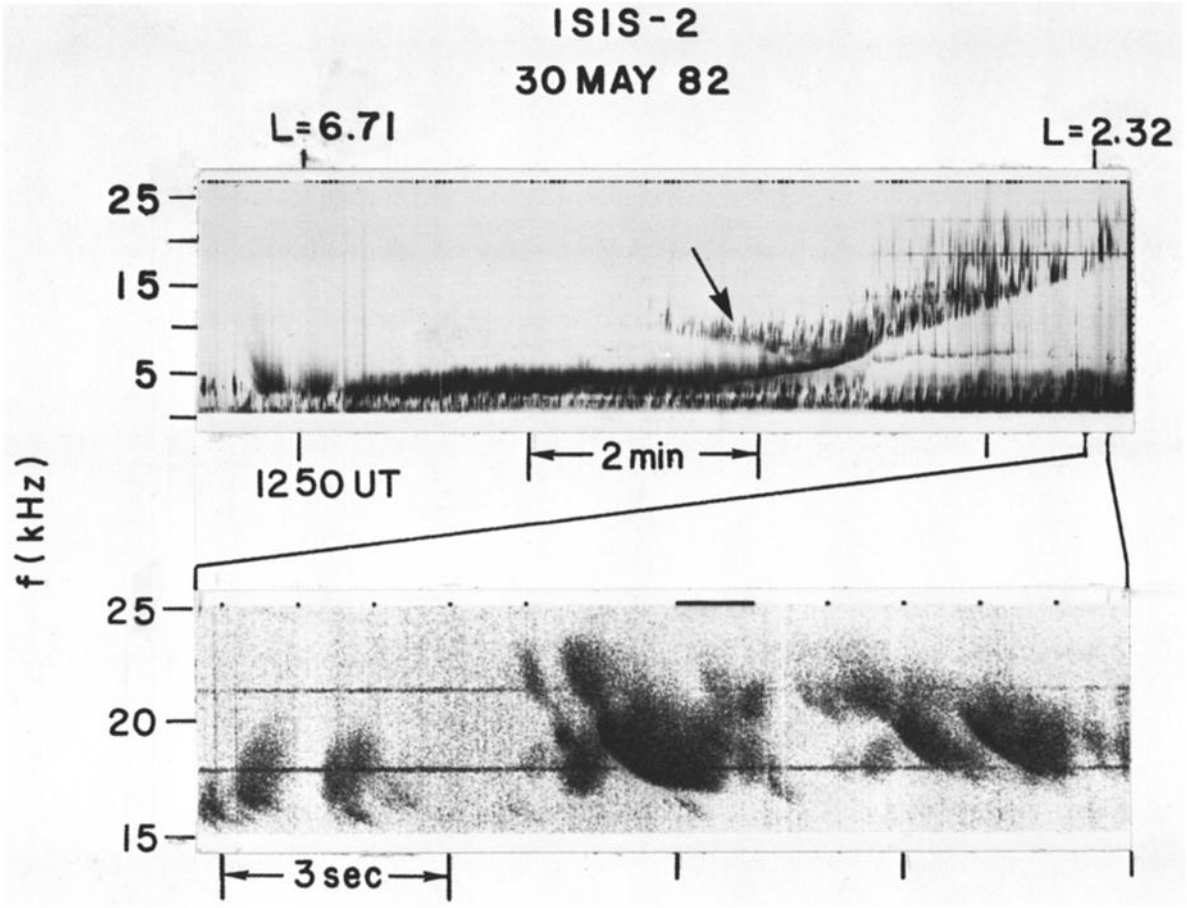

Fig. 3. Discrete emissions example observed on ISIS 2. An arrow indicates the "reflected" branch. The straight lines in the expanded spectra of the lower panel are VLF communication transmitter signals.

The observed variation of the frequency of the discrete emissions is remarkably repeatable for the cases shown, indicating clearly an L dependence of the band frequency. The measured values of the frequency of the lower edge of the band, f_l, as compared to the equatorial gyrofrequency are examined and discussed in section 3.

A rather distinct feature that is seen on June 4, 1984, is the merging of the emission band with another band in the 10- to 15-kHz range. It is hypothesized that the 10- to 15-kHz band observed in the $L \geq 3$ range may be the ionospherically reflected components of the same band observed in the $L \leq 3$ range. Better examples of these "reflected" components are seen in the low-altitude ISIS 2 satellite data discussed later. A preliminary interpretation of this "reflected" branch based on ray-tracing analysis is presented in section 3.

Plate 1 shows slightly expanded spectra of two of the cases shown in Figure 1 using a color format to illustrate the relative amplitude of the discrete emissions, as well as their frequency, as a function of time. The top panel illustrates data obtained by the 10- to 16-kHz band of the LWR on one day, while the bottom panel illustrates data obtained by the WBR (600 Hz to 10 kHz) on another day.

Figure 2 shows expanded spectra at three different times for the case of May 21, 1984, on DE 1. The middle panels show the relationship of the emission band (indicated by an arrow) to other waves in the 600-Hz to 20-kHz frequency range, while the lower panels illustrate the detailed structure of the emissions within a ~4-kHz range. The latter clearly show the discrete nature of these emissions, the bands being constituted of a succession of individual waveforms showing varying dispersion. The spacing of the individual elements is relatively uniform and small at lower frequencies (higher L shells), resulting in a "hisslike," nearly continuous, emission band. As the band frequency increases (satellite moving to lower L shells), the band seems to "break up," with emission elements occurring in bursts with irregular spacing. While Figure 2 only shows the case of May 21, 1984, the spectral characteristics on the other days shown in Figure 1 are found to be similar. Compared to chorus emissions previously observed outside the plasmasphere, the spectral shapes of the emissions appear to be more impulsive in nature with much larger df/dt slopes, and also exhibit dispersion that is unlike that of typical rising and falling chorus emissions [*Burtis and Helliwell*, 1976]. Specific similarities and differences are discussed in detail in section 3.

The higher-frequency (> 10 kHz) portions of the data shown in Figures 1 and 2 were acquired with the 10- to 16-kHz LWR receiver channel. Thus, the amplitudes at the higher-frequency (lower-L) ends of the emission bands in Figure 1 may be limited due to the receiver response. However, data from the University of Iowa sweep frequency receiver (SFR), with a frequency range of 10 Hz to 400 kHz, indicates that, for all four cases shown in Figure 1, the emission band did not extend inside $L \simeq 2.4$ (Plate 2 shows SFR data for one case). For the specific case of May 21, 1984 (Figure 2), the upper frequency limit of the band for the most intense part of the emission band is found to be ~15 kHz.

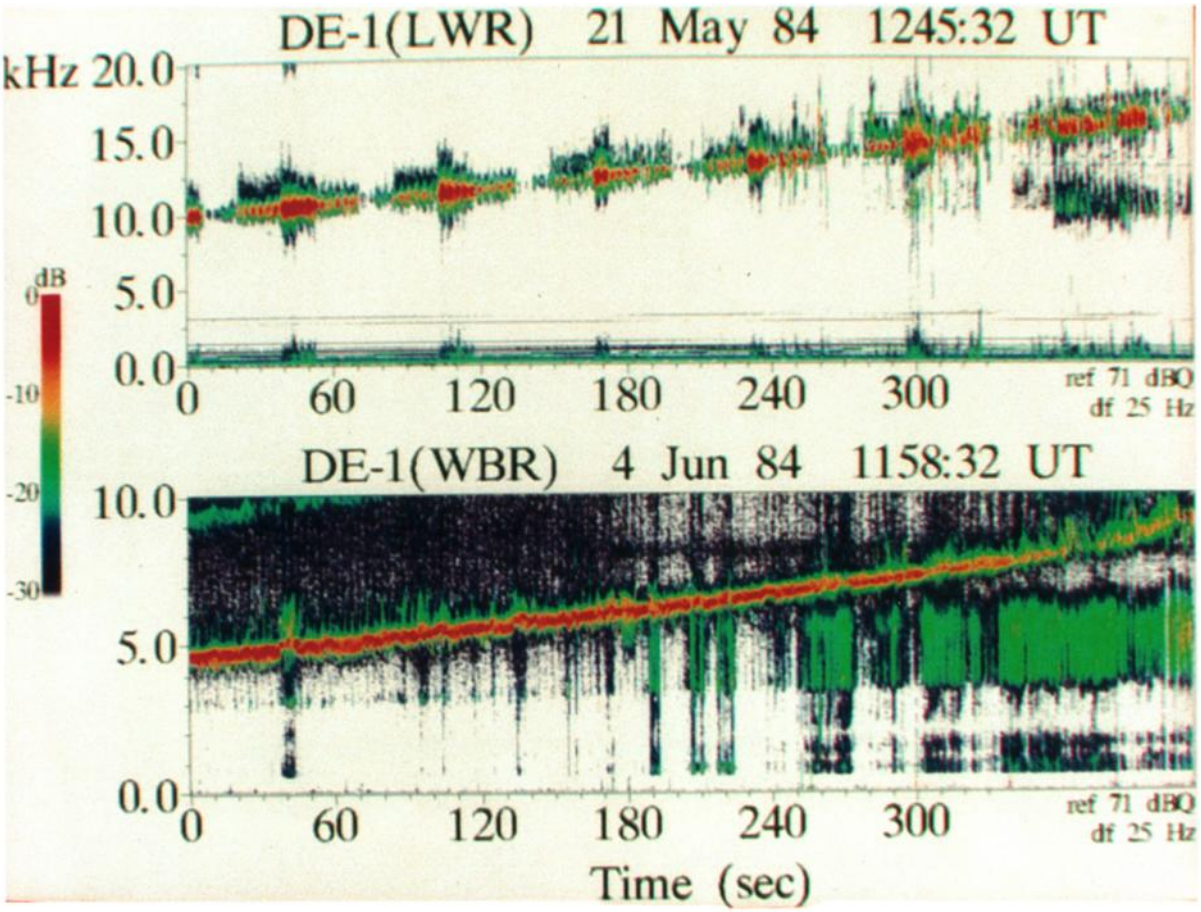

Plate 1. Two cases from those shown in Figure 1 presented in terms of color dynamic spectra to illustrate the relative amplitude, as well as the frequency, of the discrete emissions as a function of time. The bottom panel shows data from the WBR (600 Hz to 10 kHz). The top panel shows data from the 10- to 16-kHz band of the LWR.

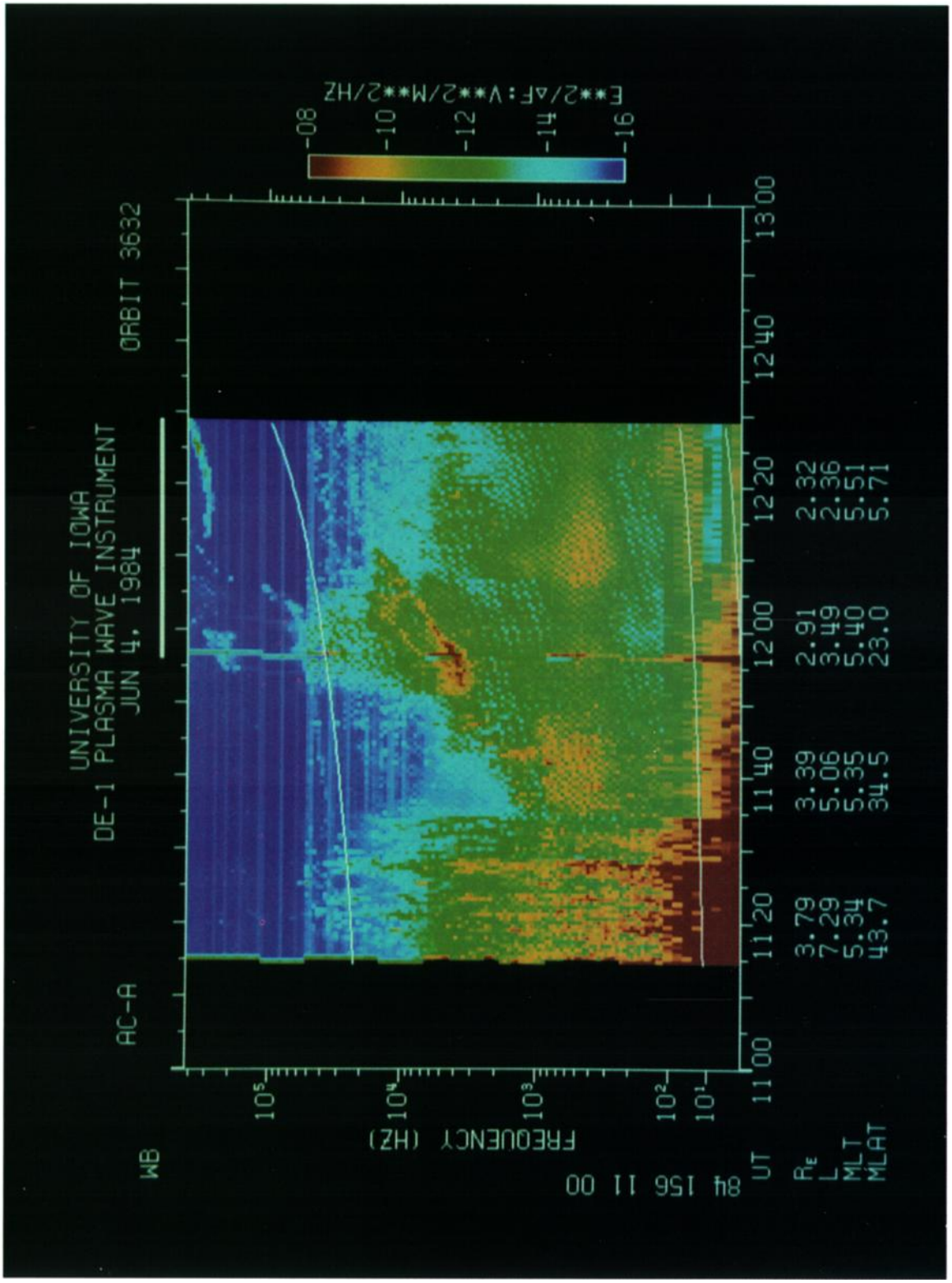

Plate 2. Data from the sweep frequency receiver (SFR) instrument showing the wave activity in the range 10 Hz to 400 kHz. The emission band is identified as a dominantly strong feature in the frequency range 2–20 kHz, observed near $L \simeq 3$. The variation of the emission band frequency with L shell is easily noticeable. The plasmapause signature reflected in the variation of the UHR noise band frequency can be seen near the top of the spectrogram. The SFR data were provided by A. Persoon by courtesy of D. A. Gurnett of the University of Iowa. The data shown were acquired using the E_x antenna.

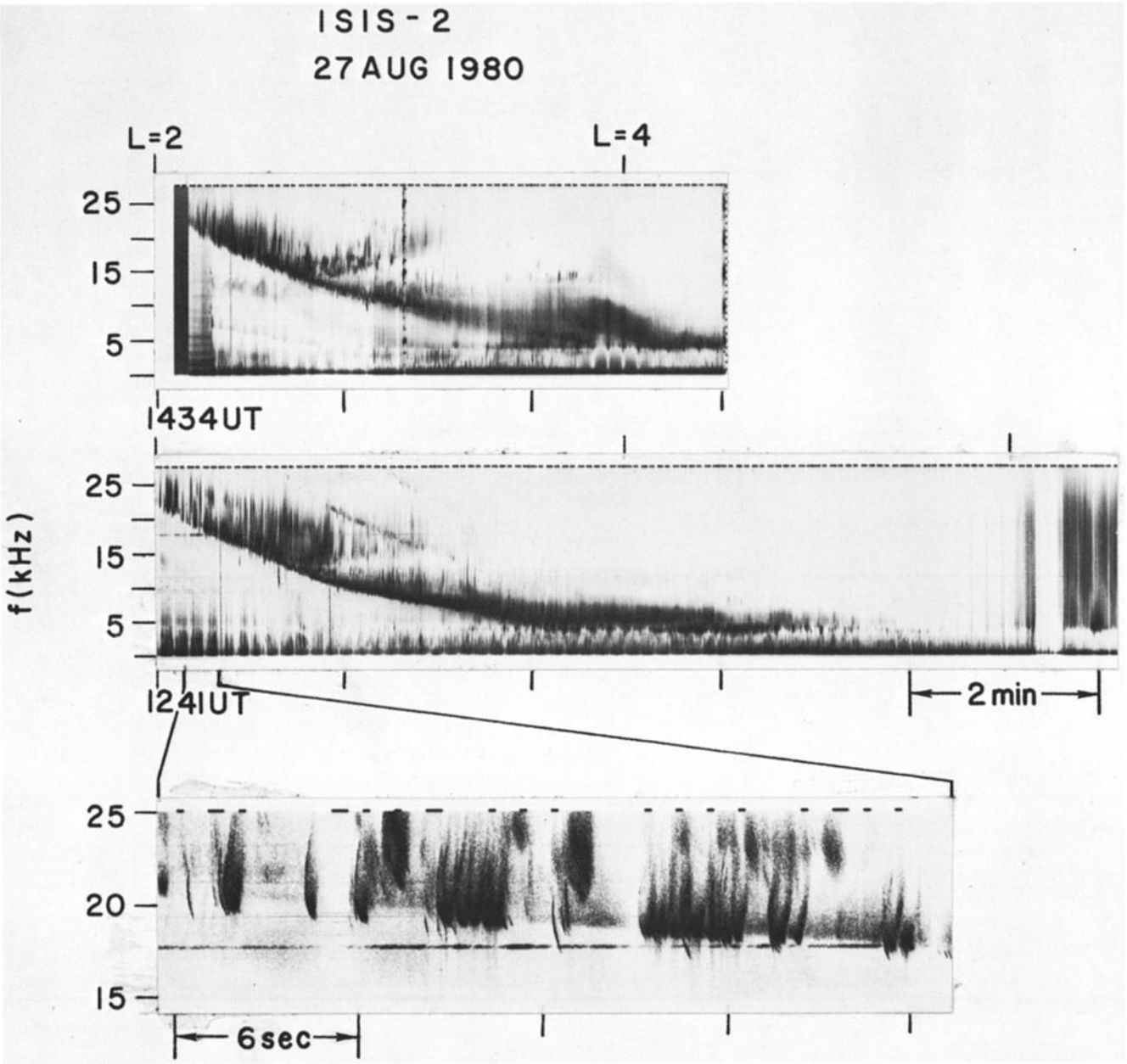

Fig. 4. Observations of discrete emissions on two successive orbits of the ISIS 2 satellite are shown in the top two panels. The bottom panel shows the expanded spectra for a selected section.

However, other data from the ISIS 2 satellite (shown later) indicate that the emission band can at times be observed on L shells as low as $L \sim 2$, with the band's upper frequency limit being ~25 kHz. The SFR data in Plate 2 also provide information on the background cold plasma density through the upper hybrid resonance (UHR) noise band that is seen near the top of the spectrogram. The plasmapause signature is clearly evident ($L_{pp} \simeq 3$); the UHR frequency increases by nearly an order of magnitude, corresponding to a density increase of a factor of ~ 100 [*Mosier et al.*, 1973; *Persoon et al.*, 1983]. We also see from Plate 2 that the emission band is observed near the inner edge of the plasmapause. This will be demonstrated more clearly with the ISIS 2 and ISEE 1 data discussed in later sections.

The nearly continuous observation of the emission band as the LWR was toggled between the E_x and B antennas (at 32-s intervals) clearly illustrates the electromagnetic nature of the waves. This is consistent with the observations of magnetospheric chorus as reported by *Burtis and Helliwell* [1976]. (In Figures 1, 2, and 7, an ~16.5-kHz interference line is present during each 32-s B antenna interval. In Figure 10, the times corresponding to the B antenna can be identified as those showing an enhanced noise background.) The absolute electric and magnetic field intensities for a specific case are discussed in a later subsection.

Spectral Properties; ISIS 2 Observations

The top panel of Figure 3 shows the broadband VLF spectrum over a 25-kHz bandwidth observed on ISIS 2. The time scale is the same as in Figure 1. An expanded spectrogram for a selected section is given in the lower panel to illustrate the dispersion characteristics of individual discrete emissions that constitute the band. The L shell variation of the emis-

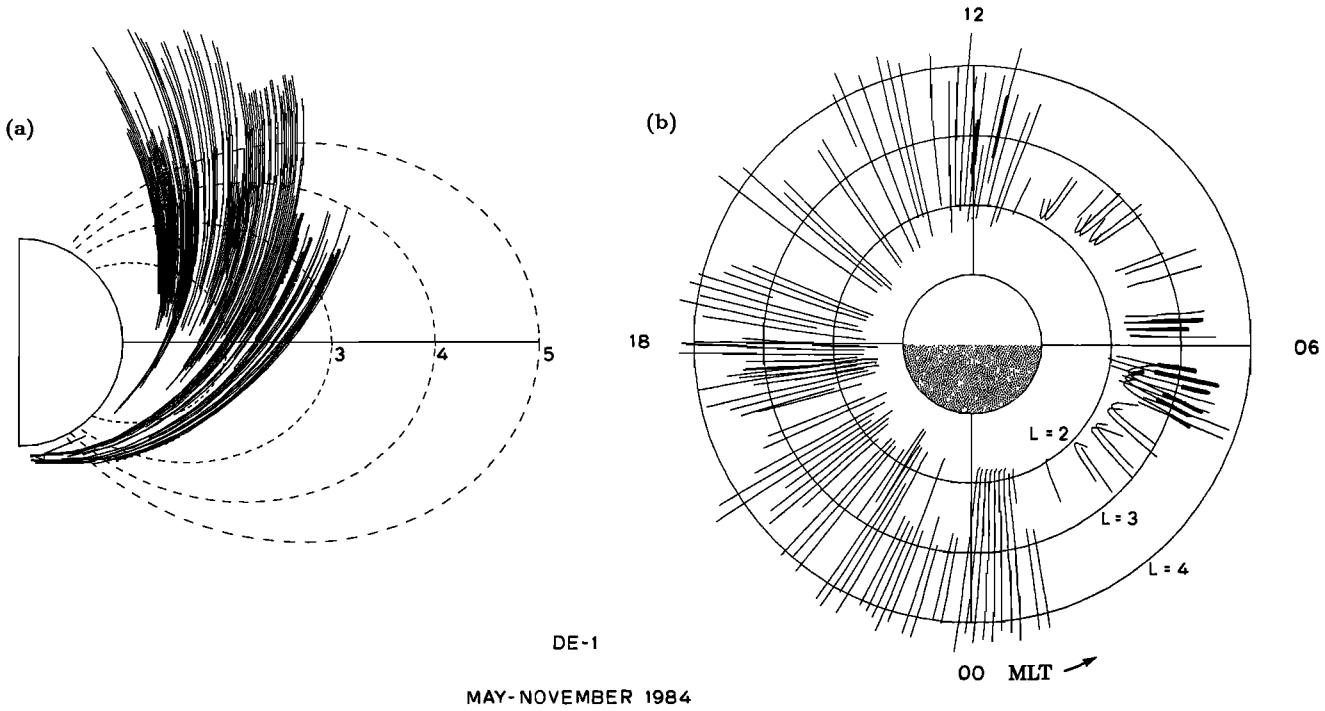

Fig. 5. (*a*) Meridional projection of DE 1 orbits on which wave data were acquired during May–November 1984. The portions of the segments where discrete emissions were observed are emphasized with heavier lines. (*b*) Local time distribution of discrete emission observations. The equatorial plane projection of the DE 1 orbits during which wave data were acquired. The portions where discrete emissions were observed are again emphasized with heavier lines.

sion band frequency for the case in Figure 3 is similar to that of the DE 1 cases shown in Figure 1. (Note that, orbiting at a lower altitude, ISIS 2 moves more rapidly across L shells.) The individual emission elements in the lower panel seem to be highly dispersed as compared to the more impulsive individual traces observed on DE 1 at higher altitudes (see Figure 2). This may be due to signal dispersion during propagation from the generation region near the equator to the low-altitude ISIS 2 satellite. However, we note that the spectral shapes of emission elements observed on different days are not always the same; detailed study of dispersion aspects of the discrete emissions is beyond the scope of the present paper and is expected to be undertaken in a later study.

The ISIS 2 data also reveal a new feature that was not clearly apparent in the DE 1 data: namely, another emission band (indicated by an arrow) that decreases in frequency with decreasing L. This new branch resembles a mirror image of the main branch and is most likely related to it. As noted above, this "reflected" branch can also be seen in the DE 1 data for June 4, 1984, shown in Figure 1.

Figure 4 shows another example of an ISIS 2 observation of the discrete emissions. The top two panels show compressed records of data acquired at Ottawa, Canada, on two successive orbits, whereas the lower panel shows the expanded spectra in a selected period. Features similar to those discussed in connection with Figure 3 are seen in the top two panels, including the "reflected" branch discussed in the previous paragraph. The fact that the emission band is observed on two successive orbits illustrates the enduring nature of the phenomenon.

Occurrence Characteristics: L Shell and Local Time Distribution

The occurrence characteristics of the discrete VLF emissions were studied using DE 1 data acquired during the pe-

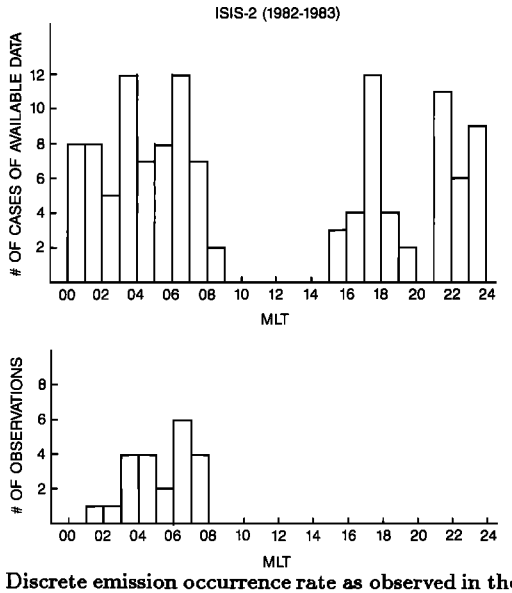

Fig. 6. Discrete emission occurrence rate as observed in the 1982 and 1983 ISIS 2 data. The top panel shows the number of cases of available data as a function of local time, whereas the lower panel shows the number of cases where discrete emissions with the reported characteristics have been observed.

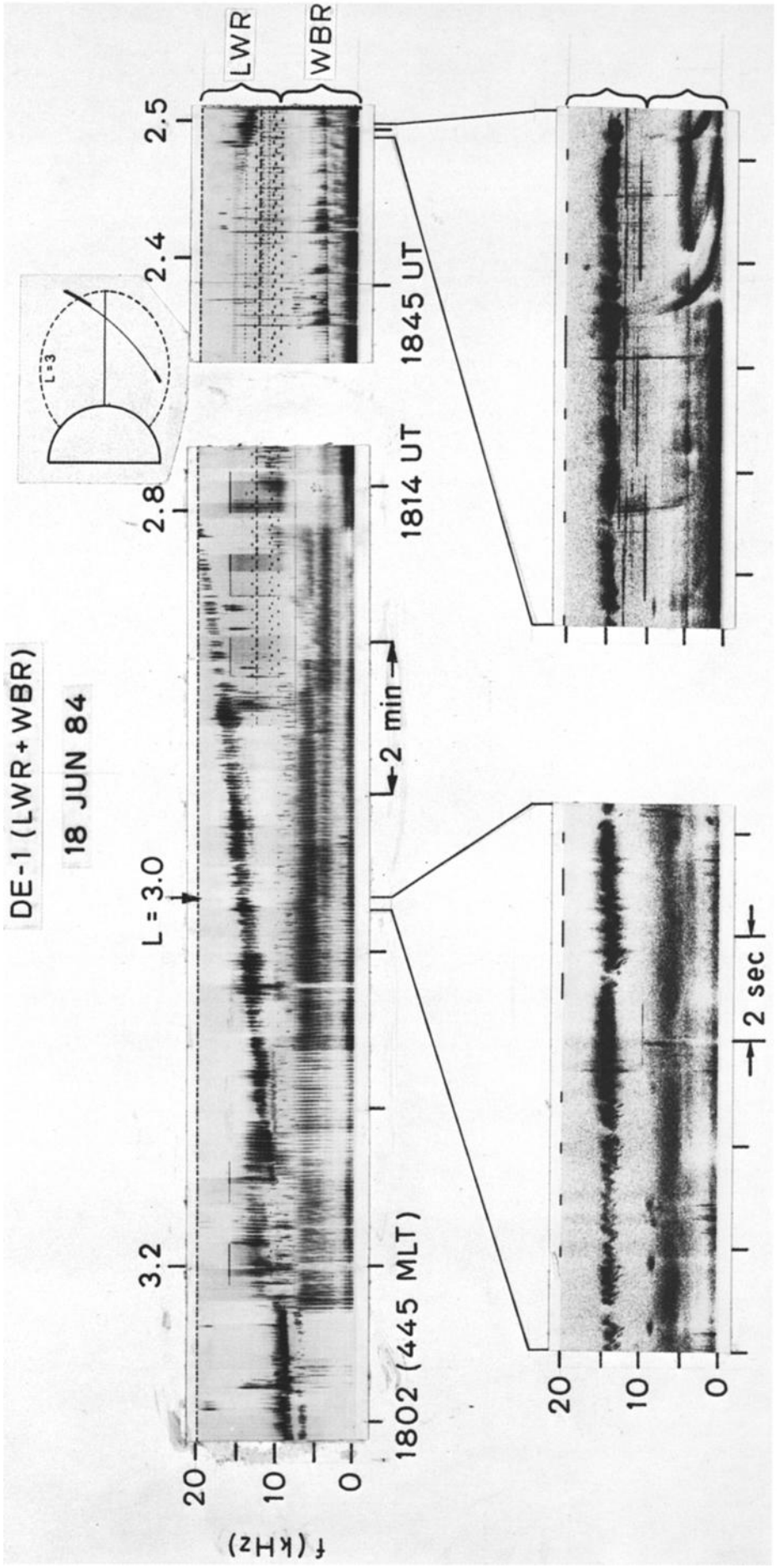

Fig. 7. Spectrogram of the discrete emissions observed on June 18, 1984. The emission band is observed successively in the northern and southern hemisphere during the same pass as indicated by the heavier lines on the inset meridional plane plot. The lower panels show the spectra on an expanded time scale.

riod May–November 1984. Figure 5*a* shows a meridional plane projection of the DE 1 orbital segments during which wave data were acquired. The thin lines indicate where data were acquired; the portions of the segments where the discrete emissions were observed are emphasized with heavier lines. An equatorial plane plot of the same orbital segments, viewed from the north, is shown in Figure 5*b* to illustrate the magnetic local time dependence. Here, the radial coordinate represents L value, and the azimuthal coordinate magnetic local time. The segments shown are the orbits as projected on the magnetic equatorial plane.

The results shown indicate that the emissions are predominantly observed in the early morning local time sector of ~0400–0700 MLT, although there also exist two cases of observations in the 1100–1200 MLT region. The L shell range of observation seems at first to be limited to ~2.4–3.6. However, the lower-frequency (higher-L) end of the band cannot be determined from the DE 1 data since, as indicated in Figure 5, the band tended to be observed as soon as data acquisition started. However, in one of the DE 1 cases, the emission band merges into and becomes indistinguishable from the lower hybrid resonance (LHR) noise band beyond $L >$ ~3.6. This characteristic is also seen in ISIS 2 and ISEE 1 data.

Statistics of ISIS 2 data for 1982 and 1983 as a function of local time are shown in Figure 6. The results corroborate the local time dependence illustrated in Figure 5 for DE 1 data, indicating that the emissions occur predominantly in the early morning local time sector. For example, in the 0600–0700 MLT period, emissions were observed in 6 out of 12 cases, whereas no emissions were observed in any of the 12 cases in the 1700–1800 MLT sector. In general, event occurrence seems to be limited to morning local time, with peak occurrence being in the 0300–0800 MLT period. However, it should be recognized that for both DE 1 and ISIS 2, limitations in data coverage preclude definite determination of the emission occurrence in the 0800–1100 local time period. *Dunckel and Helliwell* [1969] measured peak intensities of whistler mode emissions occurring from ~0600 to 1600 MLT for $2 < L < 6$. And *Burtis and Helliwell* [1976] found that the level of magnetospheric chorus activity shows little variation from 0300 to 1500 MLT. Thus, further information concerning discrete VLF emissions in the 0800–1100 local time period is needed in investigating their relationship to magnetospheric chorus.

Distribution in Geomagnetic Latitude

The data shown in Figures 1 through 5 and Plates 1 and 2 illustrate clearly that the discrete emissions are observed at near-equatorial as well as at off-equatorial locations. In one DE 1 case, on June 18, 1984, the emission band was observed in the northern and subsequently in the southern hemisphere during the same inbound pass. The data for this day are shown in Figure 7, which also illustrate the variation of the observed emission frequency with geomagnetic latitude. We note that in both of the expanded segments shown in the lower panel the center frequency of the band is ~15 kHz. However, the first segment was acquired at higher latitudes near $L \simeq 3$, whereas the second segment shows data from lower latitudes and at $L \simeq 2.5$. This finding suggests that the emissions propagated in the nonducted mode, on ray paths that were not necessarily aligned with the field lines. If the generation region is assumed to be near the geomagnetic equator, ray tracing, using density data acquired on board the satellite (i.e., UHR data from the SFR), shows that the data of Figure 7 are consistent with the inward deviation (in L shell) of ~15-kHz rays as they propagate away from the equator to lower latitudes. This is also characteristic of magnetospheric chorus [*Burtis and Helliwell*, 1976]. Sample ray paths exhibiting this behavior are presented in section 3.

Electric and Magnetic Field Intensity

The electric and magnetic field intensities of the discrete VLF emissions observed for the particular case of June 18, 1984, are shown in Figure 8. The top panel illustrates the frequency-time spectra, and the lower panel the amplitude in a 1-kHz band centered at the middle of the emission band. The LWR antenna was connected to the E_x and B antennas at the times indicated by the arrows above the upper panel. The relative electric and magnetic field intensities are indicated on the left vertical axis. The electric field intensity corresponding to 0 dB amplitude is ~ 300 μV/m, whereas 0 dB for the magnetic field corresponds to ~ 2 pT. The measured peak magnetic field intensity for the emission bursts of ~ 0.5 pT is near the range of reported intensities for magnetospheric chorus outside the plasmapause, i.e., 1–100 pT [*Burtis and Helliwell*, 1976]. The field intensities for emissions observed on other days on DE 1 are generally found to be in the few pT range.

Although simultaneous measurements of both the electric and magnetic field intensities were not made, the index of refraction can be estimated by comparing the intensities immediately before and after the switching of the antennas. In Figure 8 for example, the switch occurred when the field intensities on both antennas were near the maximum of their spin cycle. These values give an estimated index of refraction of $n \simeq 5$. Using the plasma density observed on board the satellite at this time, the index of refraction can be calculated for various wave normal angles θ using the Appleton–Hartree formula for an ordinary, whistler mode wave [*Helliwell*, 1965]. The refractive indices calculated by this means for several wave normal angles are $n \simeq 4.5$, 4.7, and 6.2 for $\theta = 0°$, 20°, and 45°, respectively. Thus, the estimated and calculated values are similar.

While further work is needed in order to determine the range of intensities for the emissions, data presented previously in Plate 2 suggest that in the region $L \simeq 2.4$–3.6, the discrete emissions represent the strongest wave activity over the 10-Hz to 400-kHz frequency range. This underscores the potential role of these emissions in the wave-induced precipitation of energetic radiation belt electrons in the few tens of keV range, as discussed further in section 3.

Relationship to Geomagnetic Activity

The top panel of Figure 9 shows the relationship of the emission occurrence as observed on DE 1 to geomagnetic activity. The lower portion of this panel shows a plot of daily ΣKp values for the period May–November 1984. Above the plot are shown (1) days on which DE 1 data were acquired, (2) observation days which occur in the 0400–0700 MLT sector, and (3) days on which the discrete emissions with the above reported spectral characteristics were observed.

Examination of the data during the May–June 1984 pe-

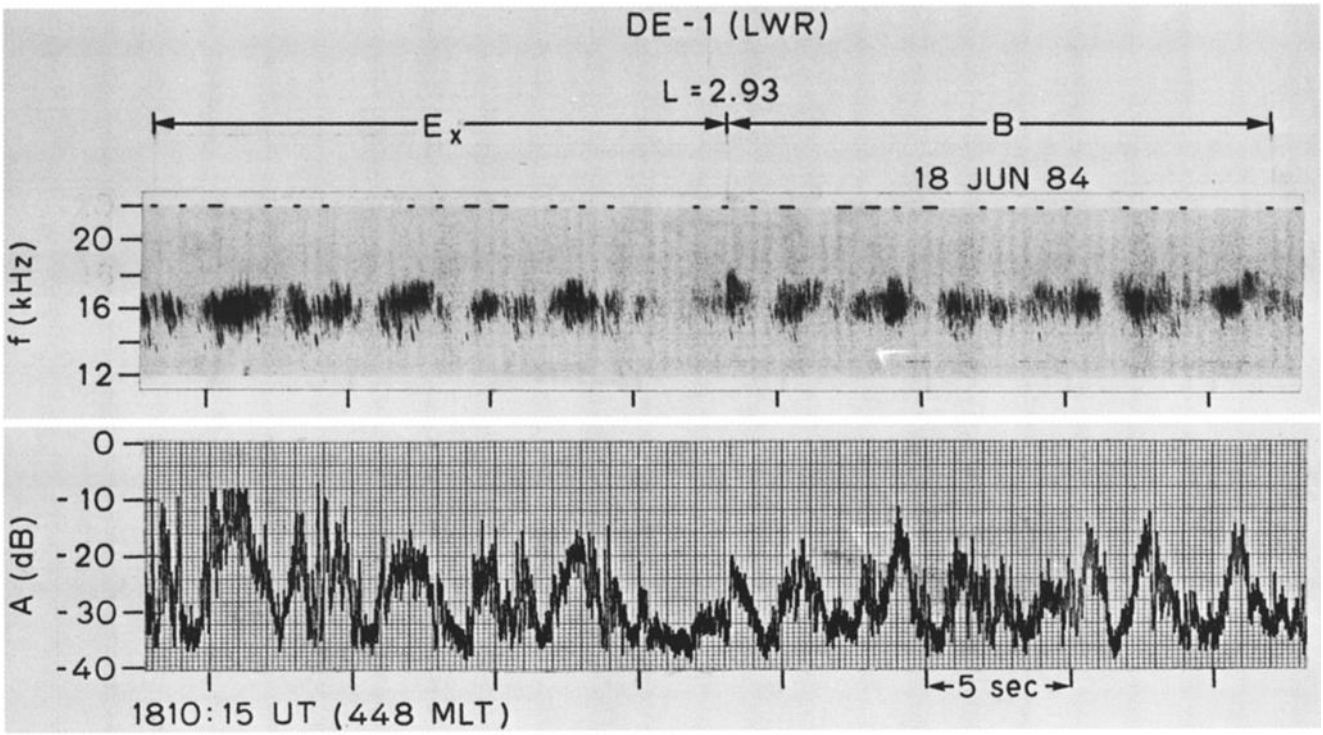

Fig. 8. Electric and magnetic field intensities of discrete emissions observed on June 18, 1984. The top panel shows the frequency-versus-time spectra, while the bottom panel shows the intensity in an ~1-kHz bandwidth centered in the middle of the emission band. The LWR is switched between the E_x and B antennas at the time indicated by the arrows.

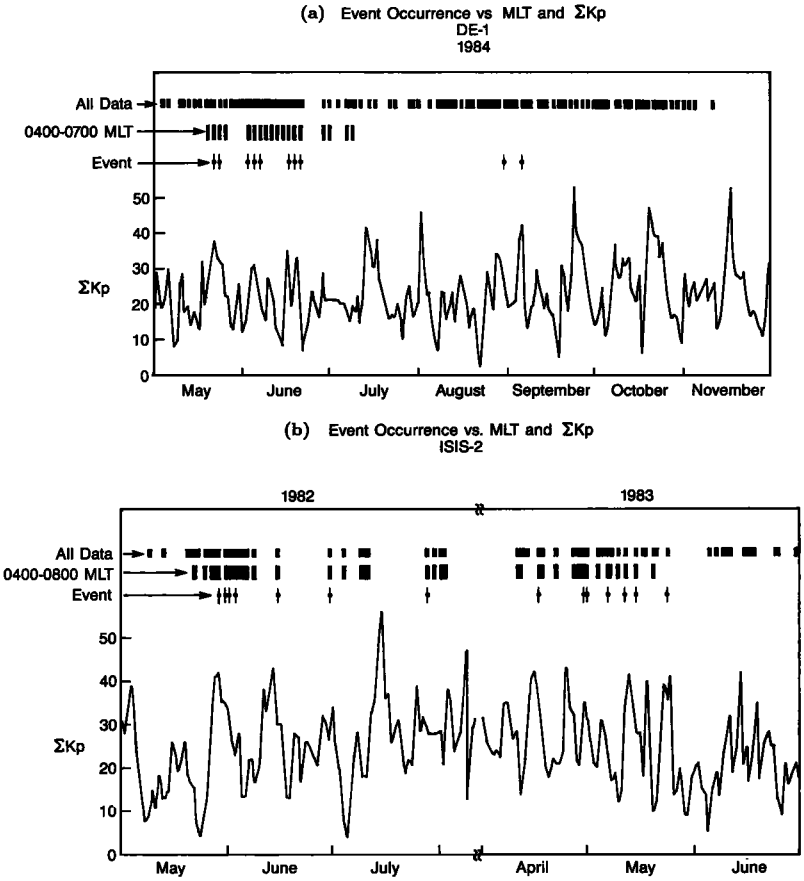

Fig. 9. (*a*) The relationship of DE 1 discrete emission occurrence to geomagnetic activity during May–November 1984. The top row indicates all days on which DE 1 data were acquired. The second row indicates days on which data were acquired during the 0400–0700 local time period. The third row indicates days on which discrete emissions were observed. Below these are plotted the daily ΣKp values. (*b*) Similar data for the ISIS 2 observations.

riod indicates that the emissions are observed whenever $\Sigma Kp > \sim 30$ and data exist in the 0400–0700 MLT period. Examples of such cases are May 21, 23, June 2, 4, 6, and June 16, 18, and 20, 1984. The phenomenon is not observed during the magnetic storm of mid-July; however, data were not acquired during the 0400–0700 MLT time period on these dates. The emission observations during the late-August–September period are during periods of high geomagnetic activity but are outside the early morning local time period. Further elaboration of these dates is given below.

The Kp dependence of the ISIS 2 observations during 1982 and 1983 is shown in the bottom panel of Figure 9 using the same format; it exhibits behavior similar to that found for DE 1. We note that emissions were observed during periods of increased activity, but generally, only if the data were acquired in the early morning local time period.

The data from both DE 1 and ISIS 2 indicate that the emissions are also seen on several days when $\Sigma Kp < 30$, as well as on a few occasions outside morning local time. These cases seem to be part of an interesting feature of the top panel of Figure 9 in which emissions tend to be observed on groups of 2–3 successive days. This suggests that once initiated, possibly as a result of increasing activity, the discrete emission band may be sustained for a few days, with gradually diminishing intensity.

This particular aspect is illustrated in Figure 10, where the emission activity on DE 1 during the three successive days of June 2, 4, and 6, 1984, is shown. Both the intensity and the occurrence rate of the individual discrete emission elements peaked on June 4, for which ΣKp for the 24-hour period immediately preceding was 35, and were much reduced for June 2 and 6, when ΣKp was 19 and 22, respectively. In fact, the emission activity seems to have been somewhat higher on June 6 than on June 2, consistent with the higher level of geomagnetic activity. Based on the gain settings of the LWR receiver, the peak emission intensity for June 6 was 29 dB lower than that of June 4 (which had peak amplitudes of ~ 145 μV/m), and the peak intensity for June 2 was 36 dB lower than that of June 4. This is qualitatively apparent from the lower panel in Figure 10, where the relatively weaker VLF transmitter signals (horizontal lines) are visible on June 2 and 6 (i.e., automatic gain setting is at a higher gain level), whereas they are not seen on June 4 (i.e., higher emission intensity has caused the gain setting to be 20–30 dB lower).

DE 1 data from several other days further illustrate the connection with ΣKp and also provide some insight into the extent of the local time regions within which the emissions may be occurring at any given time. The emissions were observed on September 5 and more faintly on August 30, which correspond to days of high geomagnetic activity (ΣKp=40, and 26, respectively); however, these events occurred in the 1100–1200 MLT sector. The relatively weak nature of the emissions observed on these days may be due to the fact that emission activity tends to be centered in the 0400–0800 MLT sector, with gradually decreasing activity in the adjoining local time regions. However, further data and analysis are needed to verify this hypothesis and establish the extent in local time of the region of occurrence.

We also note that discrete emissions were not observed on DE 1 during the late October 1984 increase in geomagnetic activity, in spite of the fact that data were acquired in the $\sim$ 0900–1000 MLT sector. The reasons for this are not clear and need to be investigated further.

Relationship to Plasmapause Location

In this section we discuss the estimated location of the plasmapause during the various times when the discrete emissions were observed on DE 1 and ISIS 2.

Since the plasmapause moves to lower L shells during periods of increased geomagnetic activity [*Carpenter et al.*, 1968] and the observation days were all during disturbed periods, a significant portion of the emission activity shown in Figures 1, 7, and 10 may in fact have occurred outside the plasmapause. Plasma density data are available for only a few of the DE 1 observation days and for none of the ISIS 2 data, but the DE 1 density data show that the plasmapause was indeed located at relatively low L shells during the observation times. In some of the DE 1 cases, the density data indicate that the emission band occurred primarily outside the plasmapause. However, emissions do extend within the plasmasphere for several of the DE 1 cases. This characteristic was pointed out previously in connection with the June 4, 1984, case shown in Plate 2. The frequency of the UHR noise band (clearly visible near the top right-hand side of the spectrogram at $\sim$400 kHz) rises suddenly at about 1205 UT ($L \simeq 3.1$), indicating the location of the plasmapause, and the discrete VLF emissions continued to be present at lower L than this. Furthermore, a change in the spectral properties of the emission was seen as the satellite moved to lower L shells at $\sim$1205:30 UT. (See the June 4, 1984, panel of Figure 1.)

Density data for the ISIS 2 examples are not available, but *Carpenter et al.* [1968] indicate that a "breakup" in the LHR noise band, involving abrupt frequency changes and transition from a smooth to an irregular appearance, frequently occurs at the plasmapause. The LHR noise band is clearly seen in Figure 11, and around the point where it suddenly changes in frequency (which is the most likely location of the plasmapause), we see changes in the spectral properties of the emissions and a merging of the "reflected" branch with the main branch. These characteristics are similar to those noted above for the June 4, 1984, DE 1 example.

A common feature of the emission band is the change in apparent bandwidth at the plasmapause; i.e., outside the plasmapause the frequency extent of the band is relatively narrow while inside the plasmapause the emission band is wide. However, the lower cutoff frequency continues to rise as the satellite moves lower in L. Amplitude measurements indicate that peak intensities of the emissions do not change significantly inside the plasmasphere, although individual elements are more separated and discontinuous inside the plasmasphere as compared to emission elements occurring outside the plasmapause.

3. INTERPRETATION AND DISCUSSION

In this section we provide an interpretation of the observations reported above. Specifically, we consider the frequency variation as a function of L shell separately for both the high-altitude DE 1 and the low-altitude ISIS 2 observations, and the gyroresonant particle energy corresponding to the observed wave frequencies. We also discuss briefly the

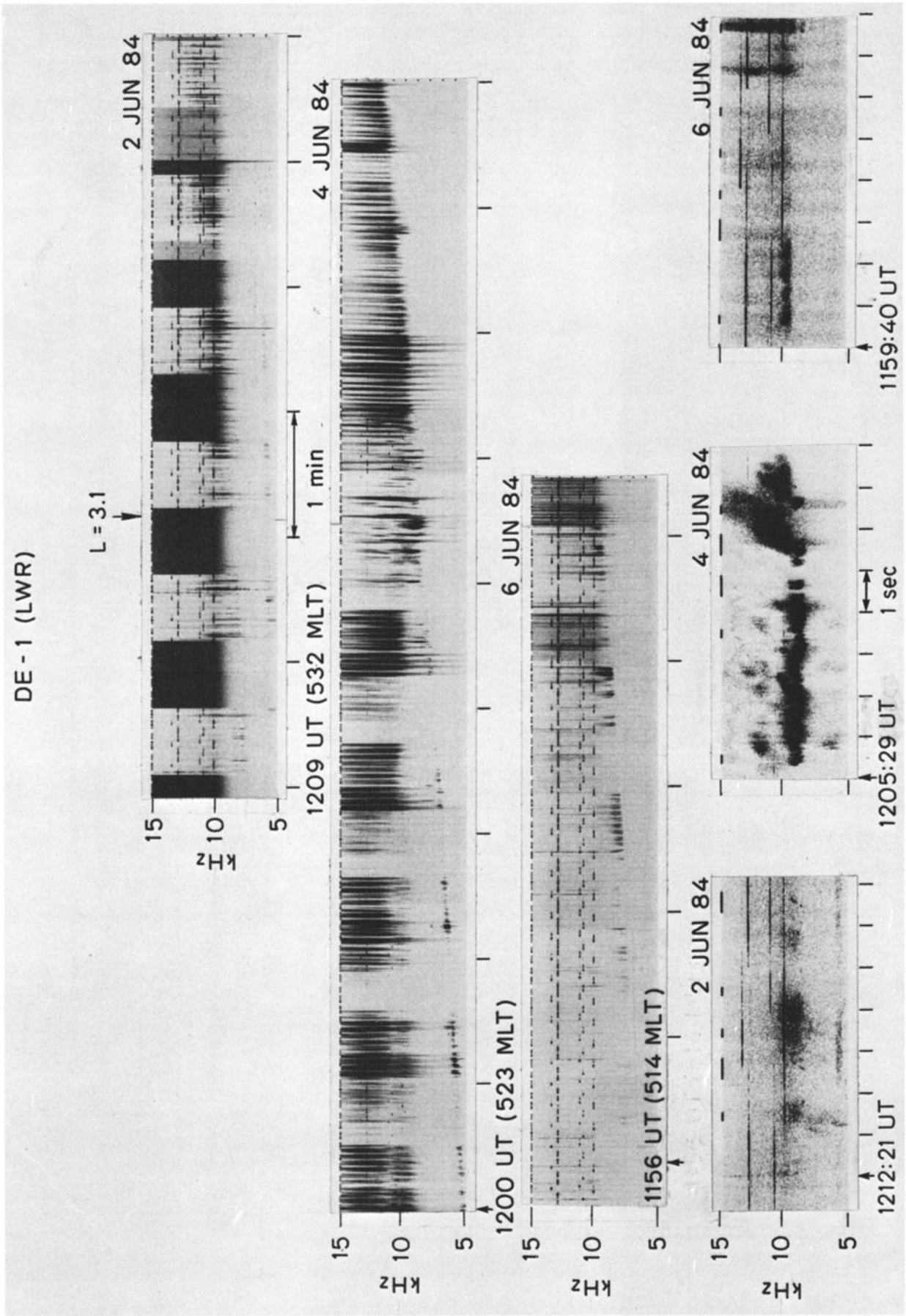

Fig. 10. Discrete emission spectra observed on June 2, 4, and 6, 1984. The expanded spectra for all three days at $L \sim 3.1$ are shown in the bottom panel. The gain setting for June 2 was 30 dB higher, and the gain setting for June 6 was 20 dB higher than that for June 4. Both the intensity and individual emission element occurrence rate peak on June 4, corresponding to a peak in geomagnetic activity ($\Sigma Kp = 35$).

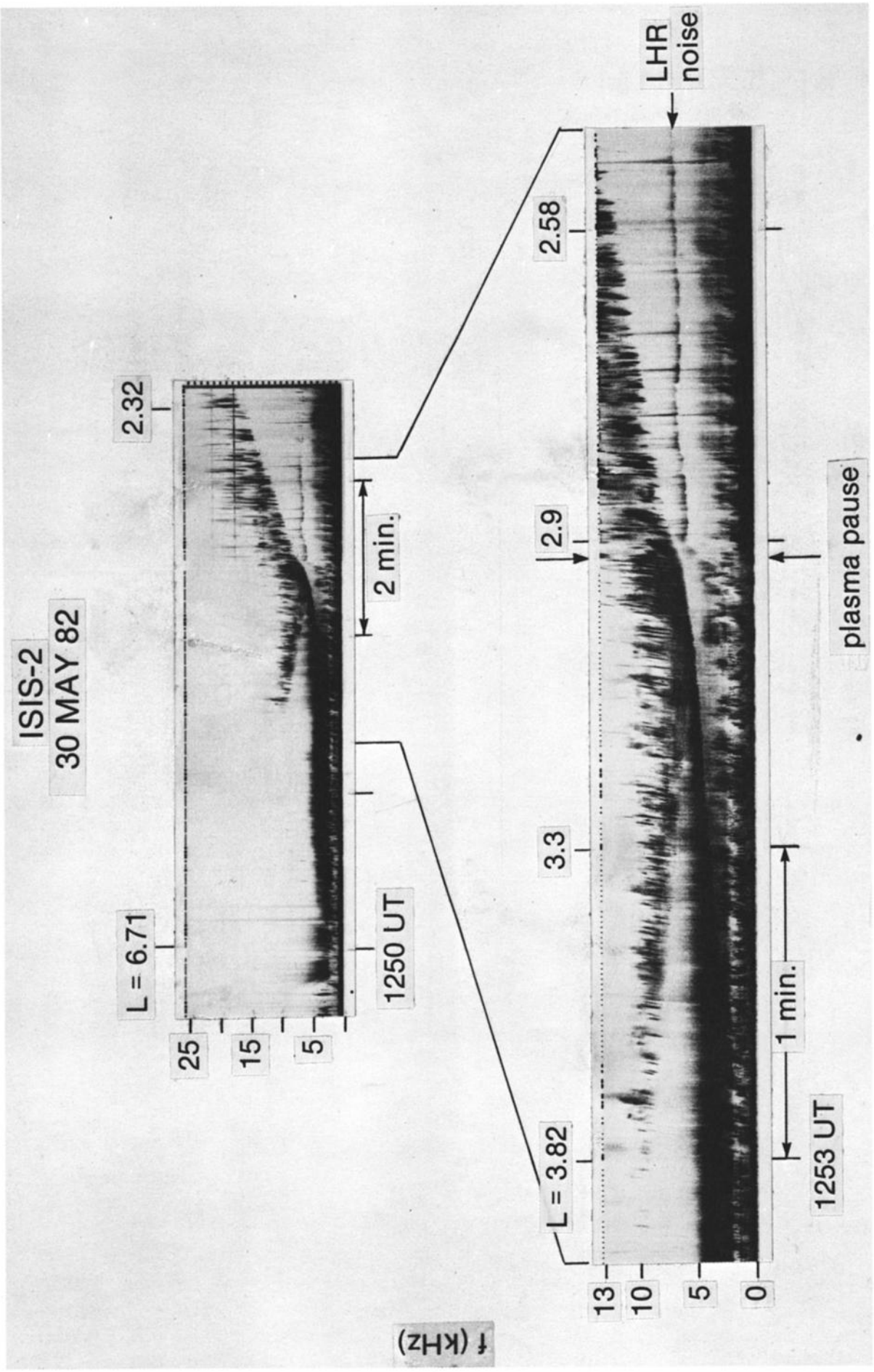

Fig. 11. Expanded spectra of the ISIS 2 observation on May 30, 1980, showing the increase in the LHR noise band frequency at the plasmapause crossing.

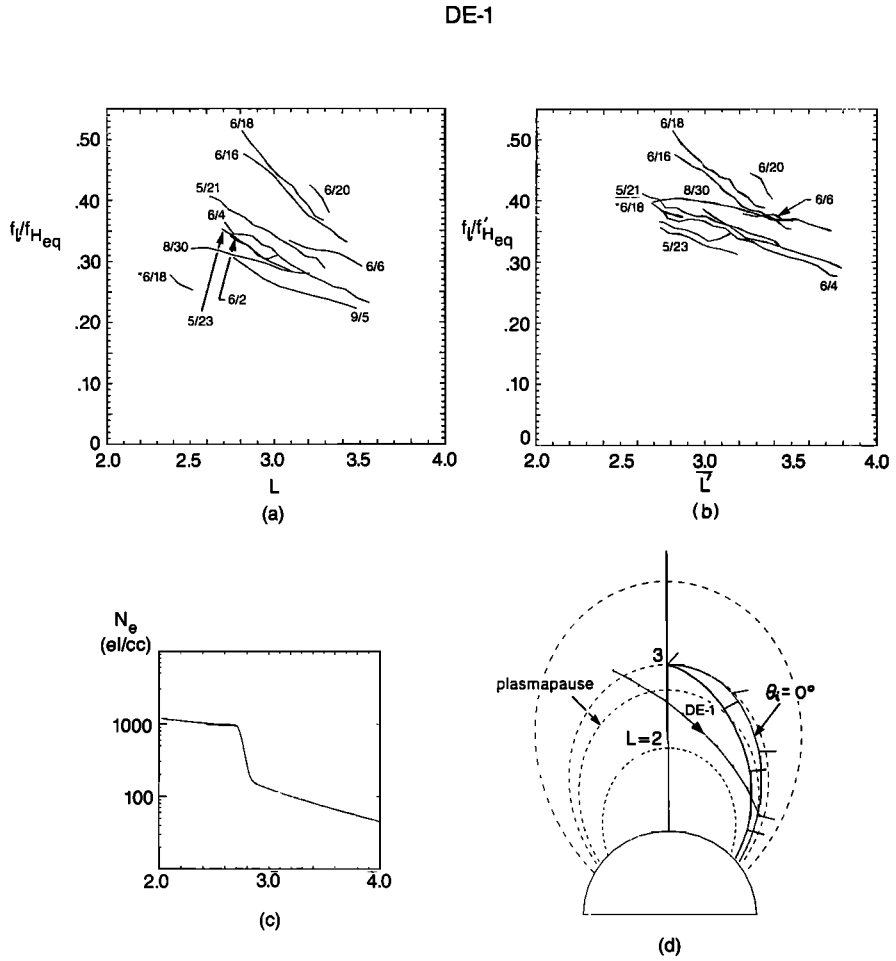

Fig. 12. (*a*) Normalized frequency f_l/f_{Heq} as a function of L, on the different days of discrete emission observation on DE 1 where f_{Heq} is the equatorial electron gyrofrequency on the magnetic field line crossing the satellite location. (*b*) Normalized frequency f_l/f'_{Heq} versus L', where f'_{Heq} is the equatorial electron gyrofrequency on the $L'=L+\Delta L$ field line, where ΔL is the deviation of the ray path from the corresponding equatorial field line on the basis of the result shown in Figure 12*d*. (*c*) The cold plasma density profile used for ray tracing. (*d*) Typical nonducted whistler mode propagation paths for a 15-kHz ray originating at the equator at $L = 3$. One ray has an initial wave normal angle of $\theta_i = 0°$. The ray that penetrates the plasmapause has a much larger initial wave normal angle.

relationship of the emissions discussed in this paper to the well-known magnetospheric chorus.

Frequency Variation; High-Altitude DE 1 Observations

A distinct feature of the emissions shown in Figures 1, 3, 4, and 7 is the variation of the emission frequency with L shell. To study this variation quantitatively, we consider the lower cutoff frequency of the emission band. This frequency is denoted as f_l and is usually a well-defined feature that can be measured with relative ease and consistency.

Figure 12*a* shows a plot of the normalized frequency f_l/f_{Heq} as a function of L for all days on which the emissions were observed at relatively high altitudes on the DE 1 satellite. Here, f_{Heq} is the equatorial electron gyrofrequency on the magnetic field line that intersects the satellite location. We see that the emission frequency observed in different cases covers a wide range, namely $f_l/f_{Heq} \simeq 0.2$–0.5. However, we note that there is a general trend toward lower values at higher L shells, so that the range of f_l/f_{Heq} at any given L shell is more limited, for example being 0.2–0.35 at $L = 3.4$. An exception to this is the one case of observation at relatively low altitudes on June 18, 1984, denoted by an asterisk in Figure 12*a* (see also Figure 7). For this case, the normalized frequency f_l/f_{Heq} is low (~ 0.26) in spite of the relatively low corresponding L value of ~ 2.4. As was also discussed in connection with Figure 7, this finding is consistent with the hypothesis that the emissions observed at low altitudes on June 18, 1984, may have been generated at higher L shells and have propagated to lower L shells due to inward deviation of nonducted ray paths.

In order to check this hypothesis quantitatively, ray-tracing analysis was carried out in a model magnetosphere using a cold plasma density profile that was derived from UHR measurements with the SFR receiver on the DE 1 satellite. A sample ray path computed on this basis for 15-kHz rays originating at $L = 3$ with an initial wave normal angle aligned with the magnetic field ($\theta_i = 0°$) is shown in Figure 12*d*. According to this, 15-kHz emissions generated near the equator at $L \simeq 3$ would be observed near $L \simeq 2.7$ when the satellite is at higher latitudes (or lower altitudes).

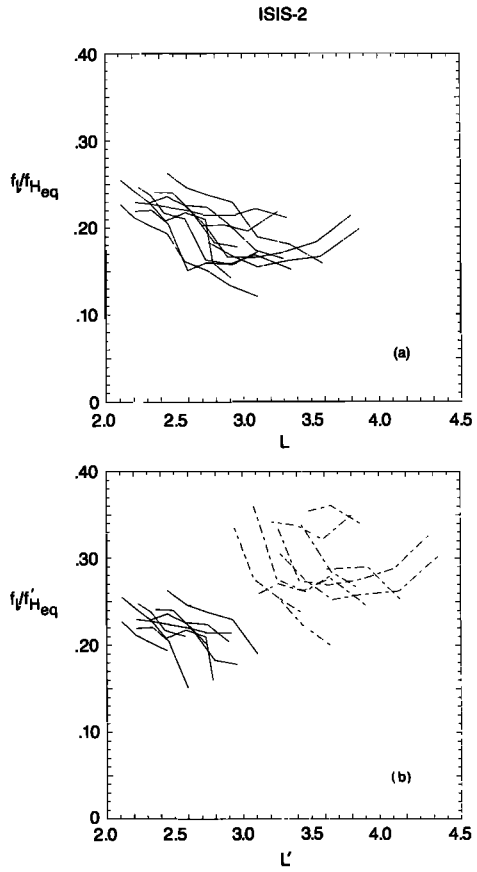

Fig. 13. (*a*) Normalized frequency f_l/f_{Heq} versus L for the ISIS 2 cases. (*b*) Dashed lines show normalized frequency f_l/f'_{Heq} versus L' where f'_{Heq} is the equatorial electron gyrofrequency on the L' field line for rays originating outside the plasmapause. The solid lines are for the portion of the discrete emissions observed within the plasmasphere and remain unchanged from Figure 13*a*.

This result is remarkably consistent with the data that were shown and discussed in connection with Figure 7.

We also note that during the period of the DE 1 observations that form part of the data base for this paper (i.e., May–November 1984) the apogee of the polar orbit of the satellite changed northward (also see Figure 5). As a result, the geomagnetic latitude at the crossing of a given L shell (e.g., $L \simeq 3$) in the northern hemisphere moved progressively to higher latitudes at a rate of $\sim 0.4°$ per day. This fact must be taken into account in comparing the variation of the emission frequency on different days, especially in view of the inward deviation of the ray paths as shown for the June 18, 1984, case.

In order to account for the inward deviation of the nonducted raypaths for the comparison of f_l/f_{Heq} on different days, we use the $\theta_i = 0°$ ray path for the June 18, 1984, case that was shown in Figure 12*d*. This is only a crude approximation since the background plasma density profile would be different from day to day; however, we note that the emission bands are observed under similar geomagnetic conditions (i.e., disturbed) and thus the differences between different days may not be as large. On the basis of this ray path, we obtain a ΔL deviation factor as a function of geomagnetic latitude and replot f_l/f'_{Heq} versus L' in Figure 12*b*, where f'_{Heq} is the equatorial electron gyrofrequency at the field line of origin (i.e., the "corrected" L shell, $L' = L + \Delta L$). The result shows that the normalized frequency variations on different days are more clustered together and (except for the group of successive days of June 16–20, which may deviate somewhat due to different propagation conditions from the other dates) the curves generally fall in the range $f_l/f'_{Heq} \simeq 0.3$–0.4. This result is quite similar to the findings of *Burtis and Helliwell* [1976], where it was found that magnetospheric chorus occurrence peaked at a frequency of $\sim 0.35 f_{Heq}$, with an additional peak at $\sim 0.6 f_{Heq}$ and a distinct gap at $\sim 0.5 f_{Heq}$. The relationship of the discrete VLF emissions studied in this paper with previously reported magnetospheric chorus is discussed below in a separate subsection.

Frequency Variation; Low-Altitude ISIS 2 Observations

While the observations of the discrete emissions on DE 1 were mostly outside the plasmapause, almost all of the ISIS 2 observations span regions both inside and outside the plasmasphere. Figure 13*a* shows a plot of the measured f_l/f_{Heq} as a function of the L shell, where L represents the field line that intersects the satellite location. We note that the uncorrected normalized frequencies of the emissions observed on ISIS 2 are generally at lower values than those for the DE 1 cases shown in Figure 12*a*, again consistent with the inward deviation of the ray paths as was introduced above. However, we note that the introduction of a ΔL correction factor to represent this deviation can only be justified for the emissions that are observed primarily outside the plasmapause, since the ray path behavior inside the plasmasphere is not likely to be similar to that outside. Furthermore, in interpreting the ISIS 2 results we need to consider the "reflected" emission branch as well as the main branch.

As mentioned in the previous section, the approximate location of the plasmapause for the ISIS 2 passes was determined on the basis of the observed increase in the LHR emission band frequency as the satellite enters the plasmasphere. As a representative case for most of the ISIS 2 observations we consider the case of May 30, 1982 (see Figure 3), where the plasmapause crossing was estimated to be at $L \simeq 2.93$. In the absence of any direct measurement of the cold plasma density we further assume an equatorial density gradient at the plasmapause that is similar to the DE 1 case for June 18, 1984 (see Figure 12*c*). The behavior of ray paths outside the plasmapause in such a model magnetosphere is very similar to that shown in Figure 12*d* for DE 1. As a result, the "corrected" f_l/f'_{Heq} versus L' can be found using the same ΔL correction as before. The f_l/f'_{Heq} versus L' obtained in this manner for the outside-plasmapause portions of the different passes are shown with dashed lines in Figure 13*b*. (The solid lines represent the portion of the emission observed inside the plasmapause for which no correction for L shell is made.) We note that this leads to a picture very similar to the DE 1 cases; namely, that the emissions generally fall in the range $f_l/f'_{Heq} \simeq 0.25$–0.4, where f'_{Heq} is the equatorial gyrofrequency at the field line of origin (i.e., the "corrected" L shell).

We now consider the observations at L values lower than the estimated position of the plasmapause. Ray paths for selected frequencies starting at different L values inside the plasmapause are shown in Figure 14. The frequency and starting L shells of the ray paths shown are selected on

the basis of agreement with the data. After consideration of different ray paths it was found that results reasonably consistent with the observations can be obtained by assuming that, inside the plasmapause, the emissions originate near the equatorial plane at normalized frequencies of $f/f_{Heq} \simeq 0.20$–0.25. The comparison of the ray-tracing results with the data is shown in Figure 14, where the bottom panel shows the ISIS 2 spectrum observed on May 30, 1982, with ray paths corresponding to the emission band frequencies at different times identified using different symbols.

Figure 14 indicates that below a certain frequency, emissions generated inside the plasmapause can reflect "under" the plasmapause out into the magnetosphere. The satellite thus "sees" these emissions as those that constitute the reflected branch described above. Emissions generated above a critical frequency are too far away from the plasmapause boundary, reflect back into the plasmasphere, and are observed at a different L than the original emission. This may account for the increased bandwidth of the signal seen inside the plasmapause.

As a further example of the consistency of the above mentioned hypothesis with the data, in Figure 15 we show the computed ray paths for a different day, August 27, 1980, where the plasmapause was at a lower L shell, namely at

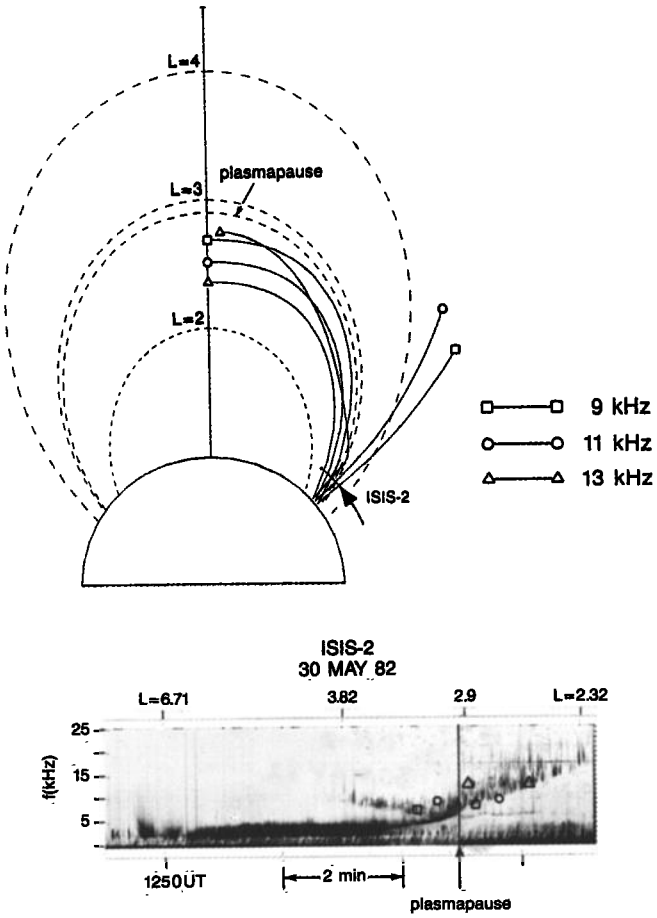

Fig. 14. Ray-tracing results for rays of three different frequencies originating inside the plasmapause ($L_{pp} = 2.9$) for the ISIS 2 observations on May 30, 1980. Symbols on the spectrogram for each of the frequencies mark representative parts of the emissions that correspond to the rays shown, and indicate a possible mechanism for the "reflected" branch.

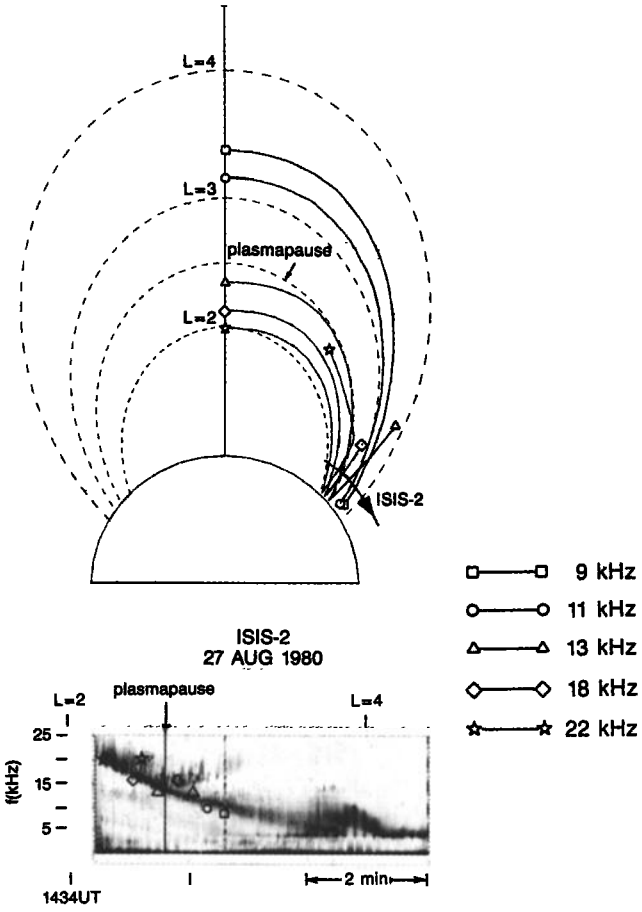

Fig. 15. Another example of ray tracing applied to ISIS 2 data for the August 27, 1980, case with the plasmapause located at a lower L shell ($L_{pp} = 2.5$) than that of Figure 14. Ray tracing indicates that frequencies which previously remained within the plasmasphere after reflection, now emerge and appear as part of the "reflected" branch. The lowest frequencies are now generated and remain outside the plasmapause.

$L \simeq 2.5$. Several differences from the previous case shown in Figure 14 are seen in the resulting ray tracing. First, the lower frequencies (represented by the 9- and 11-kHz rays) are now generated completely outside the plasmapause. Second, the critical frequency mentioned above is now somewhat higher, allowing higher-frequency rays to reflect outside the plasmapause (represented by the 13- and 18-kHz rays). However, there are still even higher frequencies that remain inside the plasmasphere.

In the June 18, 1984, DE 1 case of Figure 7, the emission observed at lower altitude and lower L ($L \simeq 2.5$) is also inside the plasmapause (which is at ~ 2.7 according to the density data for this date). The emission here does not have the same characteristics as the reflected branches on the ISIS 2 data, since the emission frequency decreases with increasing L shell. Thus, it does not seem likely that the observations on June 18, 1984, are due to a reflected branch. Rather, it appears that the waves observed at low altitudes simply penetrate the plasmapause due to their relatively high wave normal angles, in which case the ray direction is relatively independent of the local electron density [*Helliwell*, 1965]. An example of such a ray is shown in Figure 12*d*.

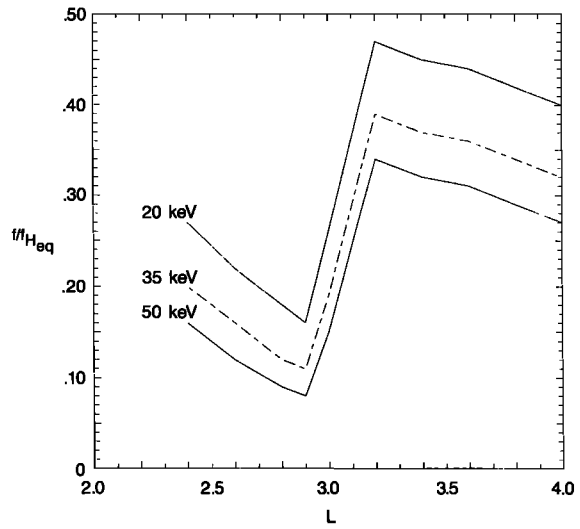

Fig. 16. Normalized frequency f/f_{Heq} calculated for waves that correspond to resonant energetic electrons with energies of 20, 35, and 50 keV using the plasma density profile measured on DE 1 for the June 18, 1984 case.

We also note that rays that penetrate the plasmapause in this manner are not expected to be observed on the ISIS 2 data due to their reflection at the LHR frequency at an altitude above the satellite. This is evident from Figure 11, where the LHR cutoff is clearly visible; waves generated outside the plasmapause and subsequently penetrating it would be at frequencies below ~ 5 kHz, which would be below the local LHR frequency at the ISIS 2 satellite location.

In summary, the above analyses indicate that the discrete VLF emission observations on the DE 1 and ISIS 2 satellites are consistent with emission generation occurring both inside and outside the plasmapause at $f/f_{Heq} \simeq 0.20$–0.25 and $f/f_{Heq} \simeq 0.3$–0.4, respectively. In the following subsection, we discuss the gyroresonant electron energies that correspond to the observed emission frequencies.

Gyroresonant Particle Energy

Assuming gyroresonant interaction with electrons near the magnetic equator as the basic generation mechanism for the observed emissions, the electron parallel resonant energy that would correspond to the observed band frequency f_l can be estimated using the gyroresonance condition:

$$\omega + \frac{n\omega}{c} v_R \cos\theta \simeq \omega_H \qquad (1)$$

where n is the whistler mode refractive index and is a function of the wave frequency ω, the wave normal angle θ, and the cold plasma density N_e, v_R is the particle's parallel resonant velocity, and ω_H is the electron gyrofrequency. Since n is a function of N_e, an independent measurement of the cold plasma density is needed in order to compute v_R (or the corresponding parallel resonant energy E_R) from (1). Measured values of N_e as a function of L are known for a few of the DE 1 observations.

Assuming that the ratio of the frequency generated to the equatorial electron gyrofrequency f/f_{Heq} (or ω/ω_H of equation (1)) is ~ 0.35 outside the plasmapause and ~ 0.22 inside the plasmapause, and assuming $\theta \simeq 0°$, values for E_R generally lie in the 20- to 50-keV range both inside and outside the plasmapause. To illustrate this better, we plot in Figure 16 the f/f_{Heq} corresponding to 20-, 35-, and 50-keV parallel resonant energy using a cold plasma density profile such as that given in Figure 12*c*. The result is consistent with the picture that emissions are generated at normalized frequencies of ~ 0.2 and ~ 0.35, respectively inside and outside the plasmapause. Thus, we are led to the conclusion that the observed discrete emissions may be generated by an enhancement of the energetic electron flux in the range between ~ 20 and 50 keV, that extends through the plasmapause into the plasmasphere. Such an enhancement is likely to occur during times of increased geomagnetic activity because of the drift of electrons into the morning sector from injection points in the nightside of the Earth [e.g., *Ejiri*, 1978]. The extension of the electrons into the plasmasphere appears to be analogous to the behavior of ring current ions in the dusk sector, as observed by *Smith and Hoffman* [1974], and probably depends upon the occurrence of injection points in the nightside at L shells lower than those typical of the dayside plasmapause. *Newell and Meng* [1986] have discussed such a relationship in explaining the introduction of $\sim$1-keV ions into the inner plasmasphere during substorms.

Relationship to Magnetospheric Chorus

In comparing the discrete VLF emissions discussed in this paper with "chorus," we begin by summarizing some of the characteristics of "typical" ELF/VLF chorus observed in the Earth's magnetosphere [*Inan et al.*, 1983; *Burtis and Helliwell*, 1969, 1976; *Tsurutani and Smith*, 1974].

1. Chorus is usually observed at $4 < L < 10$, and during the 0300–1500 MLT period.
2. The average slope df/dt of individual emission elements has values in the range 0.38 to 1.44 kHz/s in 50% of the cases.
3. Peak chorus amplitudes range from 1 to 100 pT with an average trend toward lower amplitudes at lower L shells (higher frequencies).
4. Rising emission elements are more common (77%) than falling ones (16%) and other spectral shapes.
5. The normalized chorus frequency (f/f_{Heq}) has a bimodal distribution with peaks near $f/f_{Heq} \simeq 0.35$ and 0.55, and a minimum at $f/f_{Heq} = 0.5$.

The possibility that the discrete emissions discussed in this paper may be an extension of the outside-plasmapause chorus was mentioned earlier, and indeed one of the similarities of the two types of emissions is the finding that $f/f_{Heq} \simeq 0.3$–0.4, which is very similar to the lower of the two reported peaks for chorus occurrence, i.e., $f \sim 0.35 f_{Heq}$. However, no clear evidence of the well-known $f = 0.5 f_{Heq}$ "gap" and the second peak at $f \simeq 0.6 f_{Heq}$ was found in most cases, although a second band can be faintly seen in Figures 2, 4, and 17. This second band is very weak in amplitude compared to the lower band described above, however, and has a lower cutoff frequency that lies in the range $f_l \simeq 0.49 f_{Heq}$ to $0.9 f_{Heq}$.

As a further illustration of this new type of emission seen on another satellite, Figure 17 shows data acquired on the ISEE 1 satellite at high altitudes, during a pass across the L shells of $L = 2.5$–4.5. Discrete VLF emissions are clearly visible in Figure 17, are very similar in appearance to the

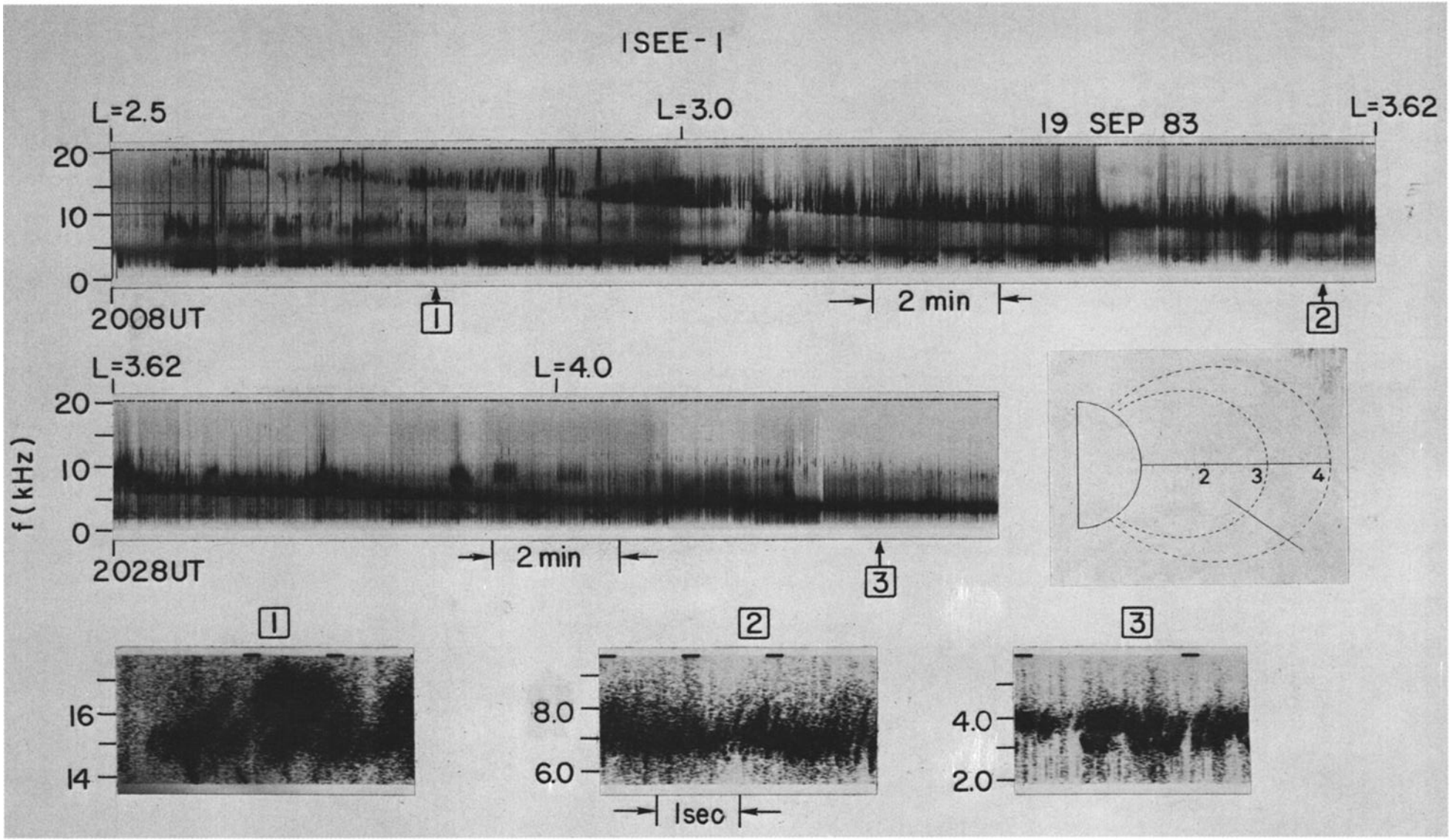

Fig. 17. Discrete emissions observed on the ISEE 1 satellite. The expanded spectra for three different segments marked 1, 2, and 3 are shown in the lowest panel. (Estimated $L_{pp} \simeq 2.9$.)

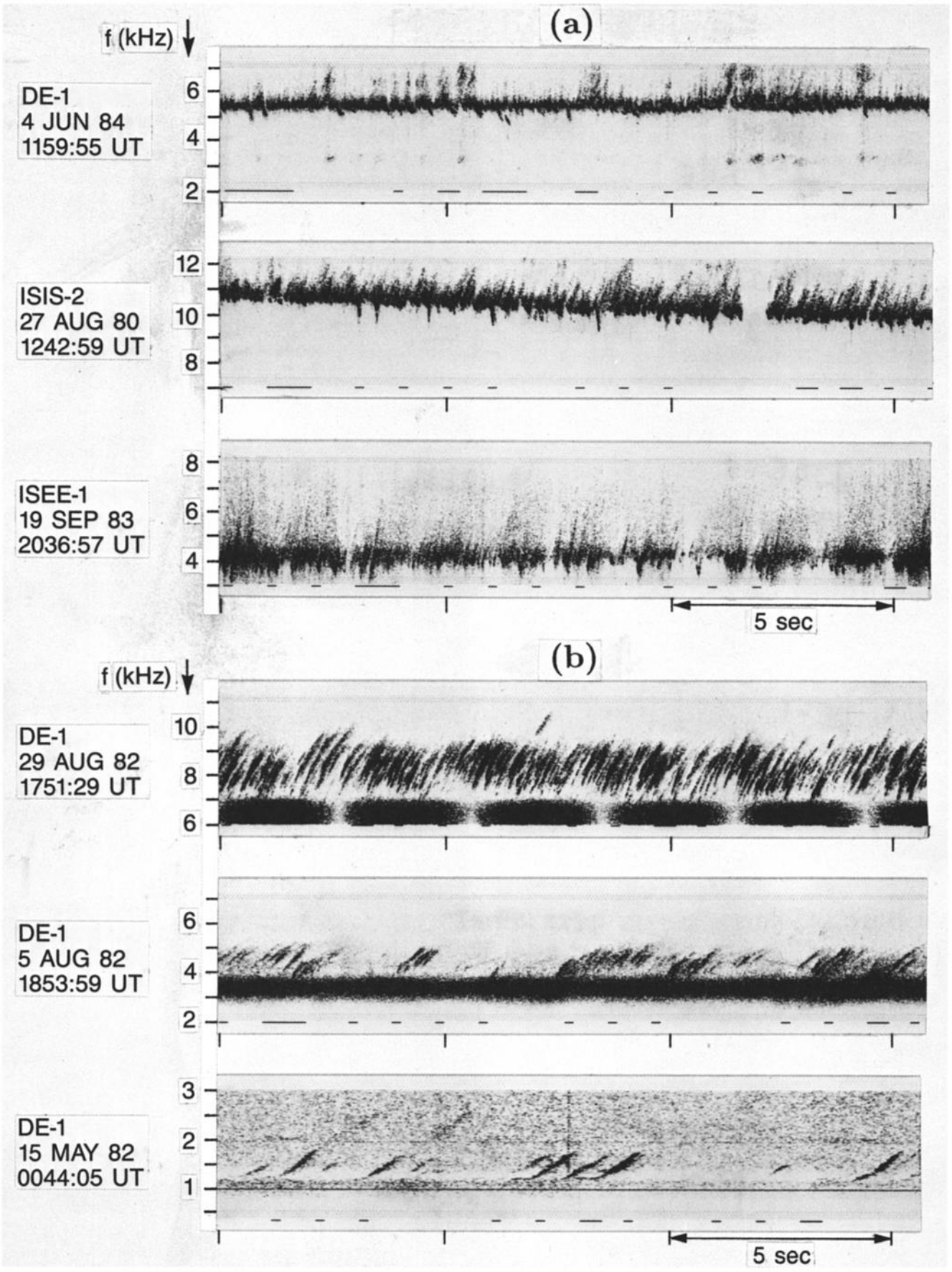

Fig. 18. (*a*) Expanded spectra of high geomagnetic activity morning time discrete VLF emissions observed on the DE 1, ISIS 2, and ISEE 1 satellites. (*b*) Expanded spectra of three different examples of typical chorus observed on DE 1. All examples are on the same time scale.

DE 1 examples, and have the characteristics discussed in previous sections. The date of the observation, September 19, 1983, is a time of significant peak in geomagnetic activity (ΣKp=41); the local time of observation is in the 0400–0800 MLT range; the variation of the emission band frequency is very similar to the DE 1 cases shown in Figure 1. The detailed spectral characteristics at three different times are shown in the lowest panel and are similar to the cases shown in the lower panel of Figure 2. The cases marked 2 and 3 are observed probably outside the plasmapause (the plasmapause location for this time was estimated to be at $L_{pp} \simeq 3.0$ using an empirical formula given by *Carpenter and Park* [1973] and altered to fit the known DE 1 data) and may be examples of classical "chorus" activity. However, the ISEE 1 data also exhibit the change in spectral character at about $L \simeq 2.9$ that is similar to the changes in the ISIS 2 and DE 1 examples of the emission at the plasmapause. Thus, the case marked 1 in Figure 17 probably was observed inside the plasmapause.

Other differences from the "typical" chorus characteristics summarized above are as follows:

1. These discrete emissions are observed in the region $2 < L < 4.5$, and during the 0400–0800 MLT period.
2. In all of the cases from the three satellites used in this paper, the slopes of the individual emission elements df/dt have values in the range of 5 to 20 kHz/s, much higher than those of "typical" chorus.
3. Measured peak magnetic field amplitudes are ≤ 1 pT.
4. Neither rising emission elements nor falling elements are predominant, and sometimes several-second periods of "risers" alternate with several-second periods of "fallers" during the same pass.

Unfortunately, in the literature, the term "chorus" has been used in an all-inclusive manner to describe a broad range of discrete emissions that are similar in appearance and general characteristics. The type of emission described in this paper has a signature that is distinct in many respects from that of magnetospheric chorus, and is observed on different passes by several satellites. To highlight these differences, Figure 18 compares expanded spectra from DE 1, ISIS 2, and ISEE 1 with several examples of typical chorus observed on DE 1. In overall general appearance these can all be termed "chorus," but the high geomagnetic activity morning time discrete emissions have spectral shapes that are distinctive at any given latitude and quite different from the typical chorus emissions shown. This figure also shows another feature of this type of emission that is not in common with typical chorus. The amplitude of an individual element of discrete VLF emission diminishes in intensity as its frequency rises, as compared to a typical chorus emission element whose amplitude remains more or less constant throughout its frequency range.

Although there are clear differences as discussed above, the similarity in normalized frequency f/f_{Heq} indicates that the underlying generation mechanism may be common to all "chorus." In any case, it is clear that further work is needed in order to establish the relationship between the new type of emissions and those that have been commonly referred to as "chorus."

4. SUMMARY

A new type of discrete electromagnetic VLF emission has been observed at middle to low latitudes inside, as well as outside, the plasmasphere. The discrete emission elements are typically confined to a bandwidth of 1–5 kHz, with the band frequency varying with L shell, being equal to $\sim$ 0.3–0.5 of the equatorial electron gyrofrequency at the estimated L shell of generation. The discrete nature of the emissions is similar to chorus observed outside the plasmasphere; however, dispersion of individual elements is often different from that of typical rising and falling chorus emissions. The phenomenon seems to occur mainly in the early morning local time sector (0400–0800 MLT) and appears to be associated with increased geomagnetic activity. The variation of the emission band frequency with L shell and latitude is consistent with an equatorial generation region and nonducted propagation to lower latitudes. Assuming gyroresonance interaction with electrons near the magnetic equator, the resonant particle energy corresponding to the band frequency is estimated to be a few tens of keV and appears to be fairly constant with L shell. There is some evidence that these emissions may constitute extensions of the well-known "chorus" into the plasmasphere; however, further work is needed in order to identify the generation regions and the generation mechanisms for the observed emissions.

Finally we note that the most striking feature of the data presented in this paper is the consistency of the phenomenon in terms of its relationship to geomagnetic activity, local time region of occurrence, and frequency variation with L. This implies that any energetic particle signatures associated with these emissions may be identifiable, even in the absence of simultaneous wave data. Such features may be detectable in the trapped particle distribution or in the form of precipitated particle signatures that would result from the cyclotron resonant interactions of these waves with energetic electrons. The latter can be observed with low-altitude satellite detectors sensitive to the 20- to 50-keV energy range, whereas the former can be detected at higher altitudes. In considering the relative contributions of these discrete emissions to the precipitation of radiation belt electrons, we note that, as shown in Plate 2, the emissions represent the strongest wave activity in the 10-Hz to 400-kHz range.

Acknowledgments. This research benefitted significantly from the many useful discussions that we have had with our colleagues in the STAR Laboratory, notably with R. A. Helliwell and D. L. Carpenter. We especially thank J. P. Katsufrakis for his early recognition of the new emission bands in the ISIS 2 data. The ISIS 2 data were made available to us by courtesy of G. James of the Communications Research Centre (CRC), Ottawa, Canada. The DE 1 wideband receiver (WBR) and the sweep frequency receiver (SFR) data (Plate 2) were made available by D. A. Gurnett of the University of Iowa, with the help of A. Persoon. The ISEE 1 data shown in Figure 17 were identified with the help of T. F. Bell. The spectrograms shown in this paper were prepared by J. Yarbrough who also conducted the search for event occurrence in the ISIS 2 data. The color presentation of the data (Plate 1) was made possible by the work of W. C. Burgess. This work was supported by the National Aeronautics and Space Administration (NASA) under grants NAG5-476, NGL-05-020-008, NAS5-25744, and NAS5-28447.

The Editor thanks R. R. Anderson and H. E. J. Koskinen for their assistance in evaluating this paper.

REFERENCES

Anderson, R. R., and D. A. Gurnett, Plasma wave observations near the plasmapause with the S^3-A satellite, *J. Geophys. Res.*, *78*, 4756, 1973.

Boskova, J., F. Jiricek, J. Smilauer, and P. Triska, VLF emis-

sions at frequencies above the LHR in the plasmasphere as observed on low-orbiting Interkosmos satellites, *Adv. Space Res.*, in press, 1987.

Burtis, W. J., and R. A. Helliwell, Banded chorus—A new type of VLF radiation observed in the magnetosphere by OGO 1 and OGO 3, *J. Geophys. Res.*, *74*, 3002, 1969.

Burtis, W. J., and R. A. Helliwell, Magnetospheric chorus: Occurrence patterns and normalized frequency, *Planet. Space Sci.*, *24*, 1007, 1976.

Carpenter, D. L., and C. G. Park, On what ionospheric workers should know about the plasmapause-plasmasphere, *Rev. Geophys.*, *11*, 133, 1973.

Carpenter, D. L., F. Walter, R. E. Barrington, and D. J. McEwen, Alouette 1 and 2 observations of abrupt changes in whistler rate and of VLF noise variations at the plasmapause—A satellite-ground study, *J. Geophys. Res.*, *73*, 2929, 1968.

Coroniti, R. V., F. L. Scarf, C. F. Kennel, and W. S. Kurth, Analysis of chorus emissions at Jupiter, *J. Geophys. Res.*, *89*, 3801, 1984.

Dunckel, N., and R. A. Helliwell, Whistler-mode emissions on the OGO 1 satellite, *J. Geophys. Res.*, *74*, 6371, 1969.

Ejiri, M., Trajectory traces of charged particles in the magnetosphere, *J. Geophys. Res.*, *83*, 4798, 1978.

Florida, C. D., The development of a series of ionospheric satellites, *Proc. IEEE*, *57*, 867, 1969.

Franklin, C. A., T. Nishizaki, and W. E. Mather, A wideband receiver for the Alouette-II and ISIS-A satellites, *DRTE Tech. Memo. 522*, Dep. of Natl. Defense, Ottawa, Canada, May 1960.

Helliwell, R. A., *Whistlers and Related Ionospheric Phenomena*, Stanford University Press, Stanford, Calif., 1965.

Helliwell, R. A., and J. P. Katsufrakis, Controlled wave-particle interaction experiments, in *Upper Atmosphere Research in Antarctica, Antarctic Res. Ser.*, vol. 29, edited by L. J. Lanzerotti and C. G. Park, p. 100, AGU, Washington, D. C., 1978.

Inan, U. S., R. A. Helliwell, and W. S. Kurth, Terrestrial versus Jovian VLF chorus: A comparative study, *J. Geophys. Res.*, *88*, 6171, 1983.

Mosier, S. R., M. L. Kaiser, and L. W. Brown, Observations of noise bands associated with the upper hybrid resonance by the Imp 6 radio astronomy experiment, *J. Geophys. Res.*, *78*, 1673, 1973.

Newell, P. T., and C.-I. Meng, Substorm introduction of $\leq$ 1-keV magnetospheric ions into the inner plasmasphere, *J. Geophys. Res.*, *91*, 11133, 1986.

Persoon, A. M., D. A. Gurnett, and S. D. Shawhan, Polar cap electron densities from DE 1 plasma wave observations, *J. Geophys. Res.*, *88*, 10123, 1983.

Poulsen, W. L., and U. S. Inan, Discrete VLF emissions at mid-to-low latitudes ($L \leq 3$), *Eos Trans. AGU*, *66*, 1039, 1985.

Shawhan, S. D., D. A. Gurnett, D. L. Odem, R. A. Helliwell, and C. G. Park, The plasma wave and quasi-static electric field instrument (PWI) for Dynamics Explorer-A, *Space Sci. Instrum.*, *5*, 535, 1981.

Smith, P. H., and R. A. Hoffman, Direct observations in the dusk hours of the characteristics of the storm time ring current particles during the beginning of magnetic storms, *J. Geophys. Res.*, *79*, 966, 1974.

Thorne, R. M., E. J. Smith, R. K. Burton, and R. E. Holzer, Plasmaspheric hiss, *J. Geophys. Res.*, *78*, 1581, 1973.

Tsurutani, B. T., and E. J. Smith, Postmidnight chorus: A substorm phenomenon, *J. Geophys. Res.*, *79*, 118, 1974.

U. S. Inan and W. L. Poulsen, Stanford University, STAR Laboratory, Department of Electrical Engineering/SEL, Stanford, CA 94305.

(Received December 12, 1986;
revised May 15, 1987;
accepted June 16, 1987.)